

Flow past a cylinder close to a free surface

By J. SHERIDAN[†], J.-C. LIN AND D. ROCKWELL

Department of Mechanical Engineering and Mechanics, 354 Packard Laboratory,
19 Memorial Drive West, Lehigh University, Bethlehem, 18015, USA

(Received 5 August 1995 and in revised form 29 May 1996)

Flow past a cylinder beneath a free surface gives rise to fundamental classes of near-wake structure that are distinctly different from the wake of a completely submerged cylinder. A central feature is the generation of a vorticity layer from the free surface due to: localized separation, in the form of small-scale breaking of a free-surface wave; or complete separation from the free surface. This vorticity layer appears adjacent to a layer from the surface of the cylinder, thereby forming a jet-like flow. It is shown that the instantaneous vorticity flux on either side of this jet is rapidly balanced immediately after the onset of separation from the free surface.

1. Introduction

Flow past a cylinder in an unbounded medium gives rise to self-sustained, limit cycle oscillations involving formation of large-scale Kármán vortices. This scenario has been the subject of intensive investigation for over half a century, and in recent years the central role of a global or absolute instability in instigating the limit-cycle oscillations has been recognized, as reviewed by Huerre & Monkewitz (1990) and Oertel (1990). The formation of these Kármán vortices can be altered, or attenuated, by a solid boundary or obstacle located adjacent to, or within, the inherently unstable near wake. When the cylinder is located sufficiently close to a solid wall, Bearman & Zdravkovich (1978) demonstrate cessation of the Kármán formation. Other techniques of passively controlling the near wake, which are less directly related to the subject of the present study, include placement of a very small cylinder in one of the separating shear layers, as investigated by Strykowski & Sreenivasan (1990), or placement of a rigid splitter plate along the plane of symmetry of the wake, as addressed by Roshko (1955), Apelt, West & Szewczyk (1973), Apelt & West (1975), and Unal & Rockwell (1987).

Very little attention has been given to the effect of an adjacent free surface on the development of the Kármán mode of instability and possible generation of new classes of the near-wake structure. For the limiting case of a cylinder piercing a free surface Triantafyllou & Dimas (1989*a, b*) demonstrate analytically that the near wake can exhibit a convective, as opposed to a global (or absolute), instability. The aim of the present investigation is to characterize the possible states of the wake when the cylinder is submerged at various depths beneath the free surface, without piercing it. This configuration is likely to generate new patterns of the near-wake structure and corresponding distortions of the free surface. Such possibilities are foreshadowed by the preliminary observation of Sheridan, Lin & Rockwell (1995), who characterized a metastable wake–wave system for a single set of parameters. For the range of potential

[†] On leave from Monash University, Melbourne, Australia.

states of the wake of interest in the present study, it is anticipated that the wake–wave structure will be generally non-stationary. It is therefore crucial to employ global, instantaneous representations of velocity and vorticity fields in defining these states.

2. Experimental system and techniques

Experiments were performed in a free-surface water channel having an inlet width of 1828 mm and a depth of 584 mm. The flow passed through two successive 3:1 contractions before entering the main test section, which had a width of 210 mm and a water depth of 527 mm. As indicated in figure 1, a cylinder of diameter $D = 25.4$ mm was mounted horizontally and adjusted to desired positions h beneath the free surface, where h is the distance from the free surface to the surface of the cylinder; it is defined in dimensionless form as $h^* \equiv h/D$. The value of h was determined at a location 150 mm upstream of the centreline of the cylinder. The vertical position of the cylinder could be varied with a high resolution, computer-controlled stepping motor located above the channel and connected to the horizontal cylinder by a rigid, vertical arm. The value of h could be resolved to within 0.5 mm.

The approach velocity U of the uniform free stream was varied over the range $236 \leq U \leq 359$ mm s⁻¹. Correspondingly, the Froude number $U/(gD)^{1/2}$ extended over the range $0.47 \leq U/(gD)^{1/2} \leq 0.72$ and the Reynolds number UD/ν , $5990 \leq UD/\nu \leq 9120$. Furthermore, the value of Froude number based on the depth of submergence h , $U/(gh)^{1/2}$, may be more representative of the flow physics; these values are defined in the figure captions. Ultimately, definition of a local Froude number based on the local velocity and free-surface height immediately above the top surface of the cylinder is most appropriate; however, these values could not be resolved in the present experiment.

Use of high-image-density particle image velocimetry (PIV) allowed determination of the instantaneous velocity distribution over the entire plane of interest. Of course, since the flow patterns addressed herein are unsteady, there will be deviations from one instantaneous image to the next, and therefore these snapshots of the flow field must be interpreted with caution in attempting to deduce the time-averaged state of the flow. On the other hand, the advantage of the present wholefield approach is that small-scale concentrations of vorticity, which are not phase repetitive with the large-scale vortical events in the flow, are typically lost during time- or phase-averaging processes and can be captured only by considering an instantaneous snapshot of the flow field.

A scanning laser version of the PIV technique, described by Rockwell *et al.* (1993), employed a scanning laser beam, originally emanating from a continuous wavelength argon–ion laser (20 W). The scanning is performed at a sufficiently high rate that each of the photographic images acquired by the camera corresponds essentially to an instantaneous snapshot. The system for generating the scanning laser sheet involves an optical train for generating a relatively small diameter beam (1.5 mm) of the laser at the mid-depth of the test section. The beam impinges upon a rotating mirror having 72 facets, which results in high-speed scanning of the beam at frequencies over the range 1250–1500 cycles s⁻¹. This value of scanning frequency allowed, first of all, generation of multiply exposed images of each particle, while the camera shutter was open; such multiple images of each particle optimize the success of the image interrogation leading to the instantaneous velocities, as described by Meinhart, Prasad & Adrian (1992). Furthermore, it ensured that the displacement between successive images did not exceed approximately 250 μ m for the characteristic flow speeds of interest here.

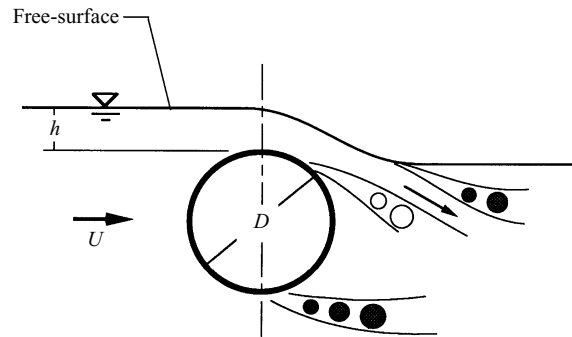


FIGURE 1. Overview of experimental arrangement and definition of flow and geometrical parameters.

Particle images were generated by seeding the flow with 12 μm diameter, metallic-coated hollow glass spheres and illuminating them with the scanning laser beam. A 35 mm Nikon F-4 camera captured the multiply exposed images of each particle. The shutter speed was typically 1/250 s, allowing three to four exposures of each particle image to be recorded on the film. In order to overcome ambiguities associated with negative velocities in regions of instantaneous reverse flow, and to minimize the dynamic range of the spacing between particles, a rotating bias mirror was located in front of the camera lens. It imparted a constant bias velocity to the entire pattern of particle images during the time the shutter was open. Selection of the proper value of bias velocity is crucial. If it is too low, it does not ensure that all velocities are positive over the region of interest; on the other hand, if it is too large, it will overshadow the actual velocities of the flow, generating substantial errors during the process of image evaluation. For the present experiments a single value of bias velocity of 360 mm s^{-1} , in a direction normal to the free stream, was found to be most effective.

The multiply exposed images of each particle were recorded on high-resolution Kodak Tmax film having $300 \text{ lines mm}^{-1}$. A camera lens with magnification of 1:3 was employed. This value of magnification provided a field of view in the plane of the laser sheet having a length of 105 mm and a width of 75 mm. Determination of the instantaneous velocity field corresponding to the recorded pattern of images required, first of all, that the image pattern be digitized at a resolution of $125 \text{ pixels mm}^{-1}$ using a digitizer. Then a single-frame, cross-correlation approach was employed to determine the velocity vector at each location of the interrogation window. The dimensions of the interrogation window were maintained at $0.72 \times 0.72 \text{ mm}^2$ on the plane of the negative, and with the magnification $M = 1:3$, the window size in the plane of the laser sheet was therefore $2.2 \times 2.2 \text{ mm}^2$. During the interrogation process, a 50% overlap of the interrogation window was maintained in order to satisfy the Nyquist sampling criterion. Such overlap therefore provided an effective grid size in the plane of the laser sheet of 1.1 mm. This interrogation and evaluation procedure yielded approximately 3500 velocity vectors in each image. Prior to evaluating the vorticity, the velocity field was mildly filtered using a Gaussian filter having a p factor of 1.3. This filtering process generated insignificant distortion of the vorticity distributions for the scales of interest.

Proper interpretation of the free-surface distortion occurring adjacent to the wake of the cylinder requires accurate determination of the surface coordinates. The coordinates of the surface were tracked using a cursor technique applied to sections of the raw digitized image, which were magnified by a factor of approximately 35:1. This technique generates the coordinates of the free surface with an estimated uncertainty

(a)

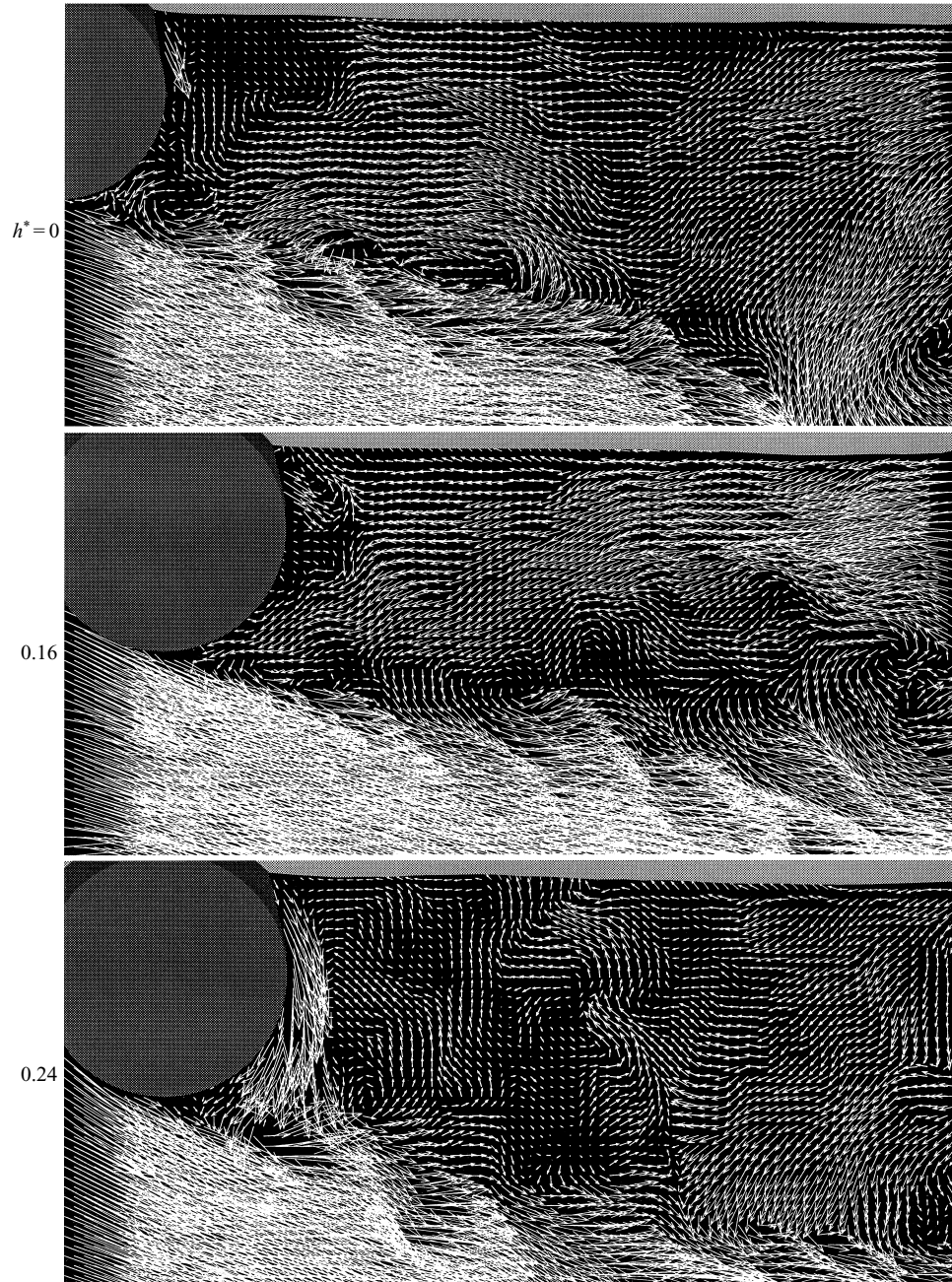


FIGURE 2(a). For caption see facing page.

of ± 0.3 mm in the physical plane of the laser sheet. Moreover, during acquisition of the images, it was desirable to incline slightly the axis of the camera lens at an angle of approximately 1.3° relative to the free surface, in order to optimize the image of the laser sheet intersection with the free surface. The effect of this inclination was determined by converting the digitized particle pattern to a pattern on an equivalent plane oriented orthogonally to the axis of the camera lens. This transformation

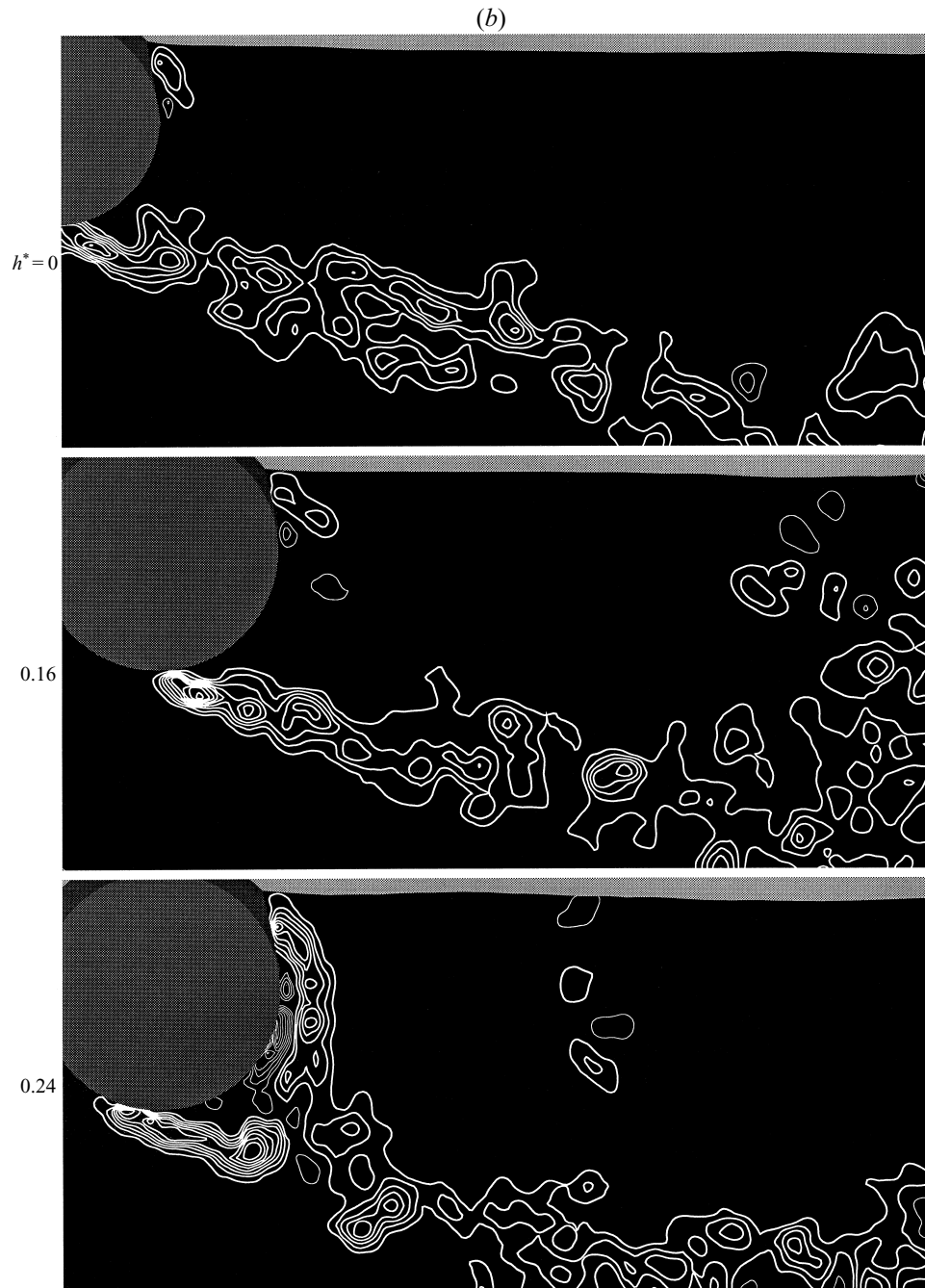


FIGURE 2. (a) Instantaneous velocity fields showing the effects of cylinder depth $h^* = h/D$ on the flow field. Depth of submergence of the cylinder increases from top to bottom. Froude number based on cylinder diameter D is $U/(gD)^{1/2} = 0.6$ for all values of h^* . Froude number based on depth of submergence $= U/(gh)^{1/2} = [U/(gD)^{1/2}] (D/h)^{1/2} = \infty, 1.5, 1.22$. Note that h is measured $5.9D$ upstream of the cylinder and does not account for local distortions above the surface of the cylinder. (b) Instantaneous vorticity fields corresponding to the velocity fields in (a). Thick contours are positive vorticity levels and thin are negative. Minimum and incremental contour levels are respectively $|\omega_{min}| = 20 \text{ s}^{-1}$ and $\Delta\omega = 20 \text{ s}^{-1}$.

function, which was subjected to simple tests of known particle displacement patterns in order to ensure its accuracy, showed that the errors in particle displacement due to inclination were of the order of 0.025%.

Owing to refraction effects of the cylinder, the scanning laser sheet did not properly illuminate the region of the flow above the top surface of the cylinder. Consequently, neither the velocity field nor the locus of the free surface could be determined in this region, which is represented in each image by a shaded, dark grey area. The upper boundary of this area was generated during image processing by swinging a constant radius of curvature from the known location of the free surface above the base of the cylinder. This boundary therefore has no physical relationship to the free surface.

On the basis of observations of the flow structure from a cylinder in the absence of a free surface, as well as observations of the flow structure from a semi-submerged cylinder, it is highly likely that the flow patterns will exhibit a degree of three-dimensionality. Although no attempt was made to characterize these patterns in the present study, qualitative observations of separation and reattachment lines, in accord with distortions of the free surface, suggest that the predominant features are, however, quasi-two-dimensional.

3. Basic states of wake

In order to determine the basic classes of flow structure in the near-wake, experiments were carried out at a sufficiently low value of Froude number Fr such that distortions of the free surface were negligible over nearly the entire range of interest. The depth of submergence h , defined in figure 1, was varied in small increments in order to determine the values that exhibited major changes in the near-wake patterns. Then, PIV images were acquired at these critical values of h , represented in dimensionless form by $h^* = h/D$. In general, it was observed that small changes of h^* could induce radical alterations of the near-wake patterns that, in all instances, were distinctly different from the wake structure of a fully-submerged cylinder.

Figures 2(a) and (b) show instantaneous distributions of velocity and vorticity for small values of submergence h^* . At $h^* = 0$, a mixing layer forms from the bottom surface of the cylinder. The swirl patterns of velocity vectors and closed contours of vorticity suggest identifiable, small-scale structures arising from the Kelvin–Helmholtz instability. A low-velocity, jet-like flow is evident between the upper surface of the cylinder and the free surface. It is dominated by positive (thick lines) vorticity originating from the free surface; positive vorticity corresponds to counterclockwise rotation of a vortical structure, i.e. a vector coming out of the paper. This jet-like flow issues into a very low-velocity region of quiescent fluid adjacent to the free surface.

At $h^* = 0.16$, the overall pattern of the wake is generally similar, except that the details of the jet-like flow and the region immediately surrounding it take on a different form. The angle of the jet with respect to the surface is smaller and a localized recirculation region occurs between the jet and the free surface. Considering the patterns at $h^* = 0$ and 0.16 together, it should be noted that they occur intermittently at both values of h^* and represent the incipient state of formation of a stable, well-defined jet from the upper surface of the cylinder, as described below. An additional feature evident in both of the velocity images at $h^* = 0$ and 0.16 is the substantial magnitude of the counterflow in the upstream direction between the free surface and the mixing layer from the bottom surface of the cylinder. This counterflow is necessary in order to satisfy the entrainment demands of the mixing layer. It is associated with formation of a large-scale recirculation vortex shown at the lower right-hand corner of

both velocity images. This type of complex flow pattern in the near-wake is associated with a substantial, downward deflection of the mixing layer formed from the bottom surface of the cylinder. It is inclined at an angle of approximately 10° with respect to the horizontal, in contrast to the mixing layer formed from the corresponding fully submerged cylinder over this particular range of Reynolds numbers, as described by Lin, Towfighi & Rockwell (1995).

A small increase in the level of submergence of the cylinder to $h^* = 0.24$ produces an abrupt onset of a jet-like flow about the base of the cylinder. The magnitude of the jet velocity is now large, having the same order as the free-stream velocity of the approach flow. Of course, this flow is not a 'jet' in a traditional sense, where the sources of vorticity on either side of the jet are from solid surfaces corresponding to the interior of the jet nozzle. Rather, the positive (thick lines) vorticity layer originates at the free surface and the negative (thin lines) layer from the top surface of the cylinder. Nevertheless, we shall loosely refer to this flow system of vorticity layers as a jet. For the vorticity distributions represented in figure 2(b), the positive vorticity emanating from the free surface dominates that generated from the surface of the cylinder. In fact, the mixing layer in the downstream region of the flow is dominated by the combined positive vorticity from the free surface and the lower surface of the cylinder.

Comparison of the vorticity distributions for all three images of figure 2(b), corresponding to $h^* = 0$ to 0.24 , shows, for locations downstream of the cylinder, that the locus of positive (thick line) vorticity is similar for all values of h^* . The formation of the jet at $h^* = 0.25$ appears, however, to cause a reduction in the counter (reverse) flow between the free surface and the mixing layer. Apparently, the entrainment demands of the initial regions of the mixing layer from the bottom surface of the cylinder are at least partially satisfied by the jet flow.

As illustrated in figures 3(a) and 3(b), further increase in the cylinder submergence to $h^* = 0.31$ generates the next state of the near wake, namely detachment of the jet from the surface of the cylinder. Two regions of large-scale swirl are suggested by the patterns of velocity vectors: a clockwise one bounded by the jet and the mixing layer from the bottom surface of the cylinder; and a counterclockwise pattern on the opposite side of the jet. The central portions of these large-scale swirls, however, have relatively low levels of vorticity. The well-defined layers of positive and negative vorticity from the free surface and top surface of the cylinder have peak vorticity levels of the same magnitude. They merge with the positive layer from the lower surface of the cylinder. Further downstream, only positive vorticity is evident; the slope of the velocity distribution defining the mixing layer is compatible with only positive vorticity.

This basic pattern maintains its general form when the submergence of the cylinder is increased to $h^* = 0.43$. The location of the jet merging with the mixing layer, however, is displaced further downstream, corresponding to the middle row of images of figures 3(a) and 3(b). Moreover, as indicated in the velocity plot, the swirl between the jet and the base of the cylinder no longer exists and the counterclockwise swirl beneath the free surface has moved downstream such that it appears along the right-hand side of the velocity image. This large-scale vortical motion involves significant vorticity, a portion of which is evident adjacent to the right margin of figure 3(b) ($h^* = 0.43$). All of these features are associated with an upward deflection of the jet, such that the angle between its axis and the free surface decreases significantly, setting the stage for an eventual attachment of the jet to the free surface.

Finally, at the largest depth of submergence $h^* = 0.75$, the jet is attached to the free surface; correspondingly, a long-wavelength distortion of the surface occurs. Since

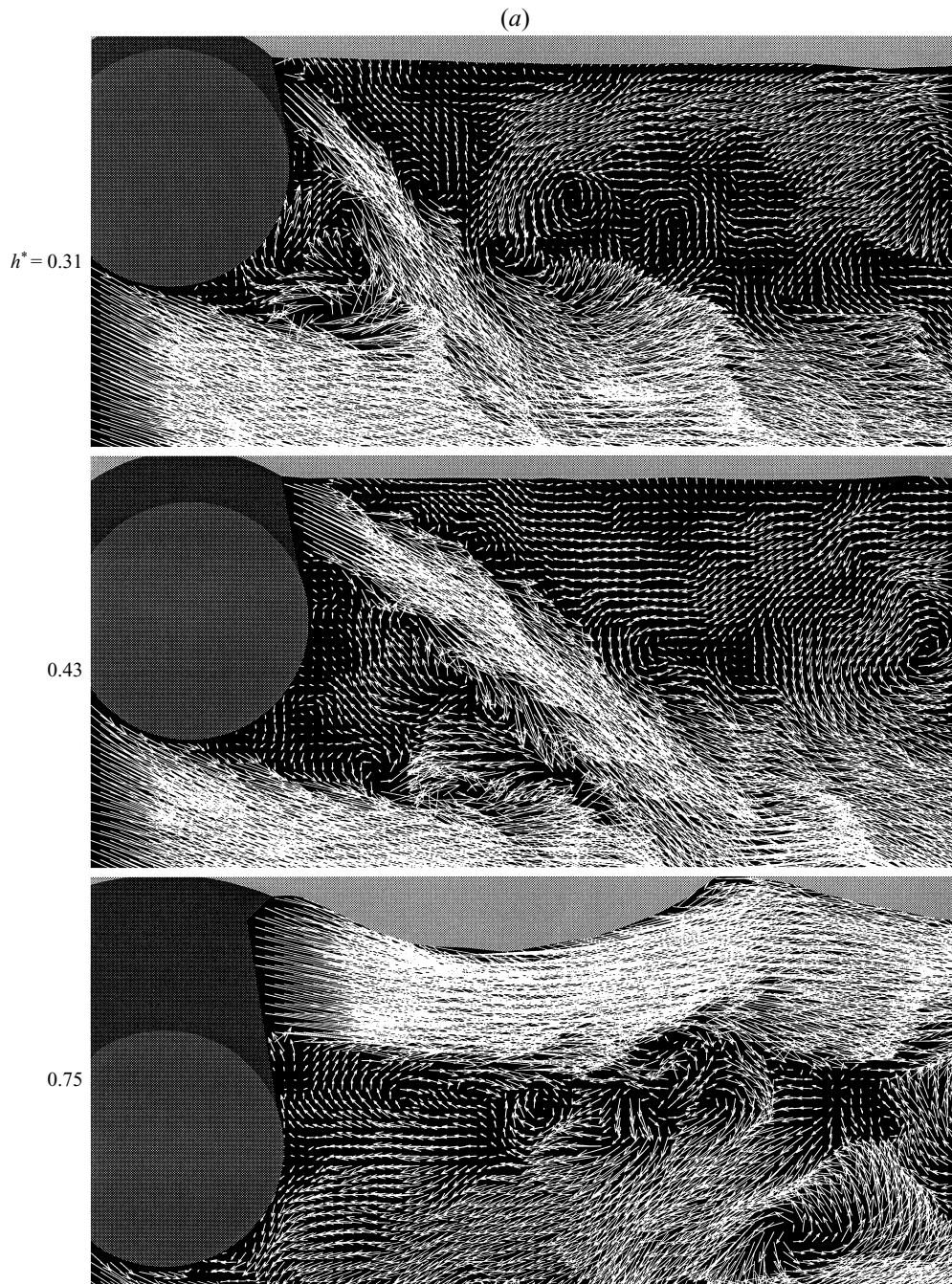


FIGURE 3(a). For caption see facing page.

separation from the free surface does not occur, there is no longer generation of a well-defined layer of positive vorticity. The trajectory of the layer of negative (thin lines) vorticity from the top surface of the cylinder is generally parallel to the locus of the free surface, and large-scale vortical structures are eventually formed in the layers from the top and bottom surfaces of the cylinder, evident by comparison of the swirl patterns

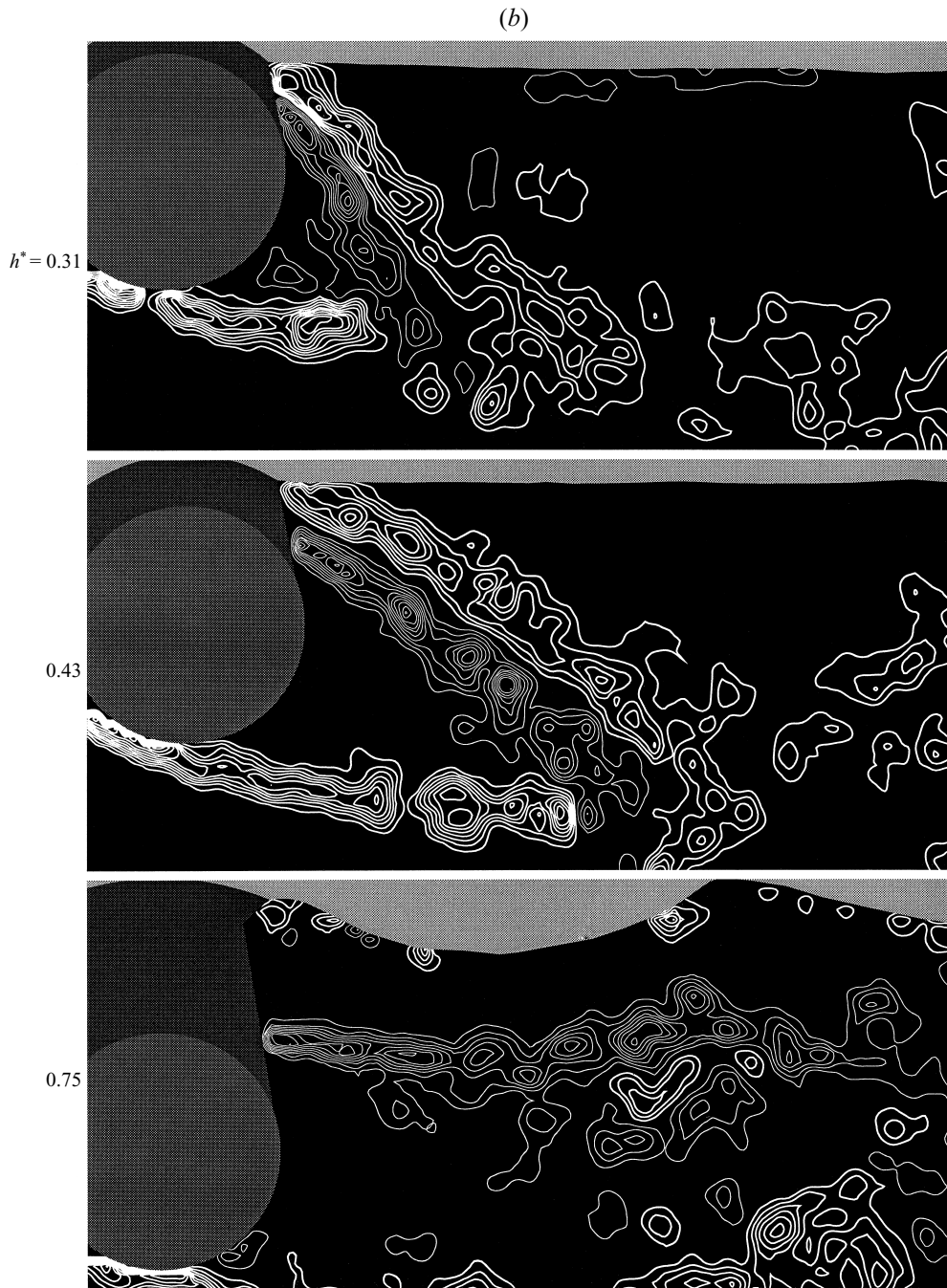


FIGURE 3. As figure 2 but for larger value of h^* . Corresponding values of $U/(gh)^{1/2} = 1.07, 0.91, 0.69$.

of velocity vectors in figure 3(a) and the clusters of vorticity concentrations in figure 3(b). The large-scale vortex in the negative (thin lines) vorticity layer is formed just ahead of the crest of the free-surface wave. These large-scale structures occur at a substantially larger distance from the base of the cylinder than for the corresponding

(a)

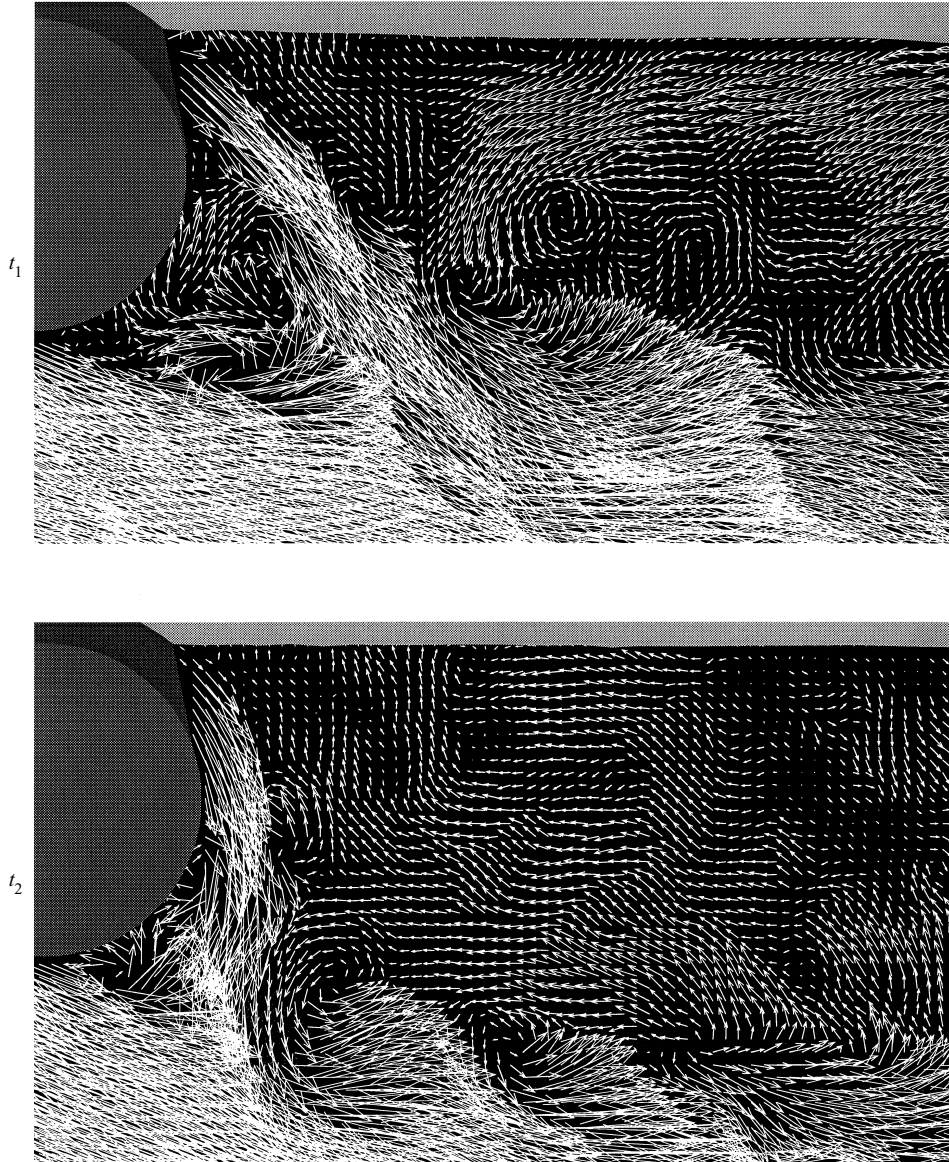


FIGURE 4(a). For caption see facing page.

case of the completely submerged cylinder, as described by Lin *et al.* (1995). The proximity of the free surface initially retards the onset of large-scale vortex formation, but subsequent development of the vorticity layer leading to large-scale vortex formation appears to be coupled to the free-surface distortion. In turn, the development of the vortex in the positive (white) layer from the cylinder may be coupled with these events.

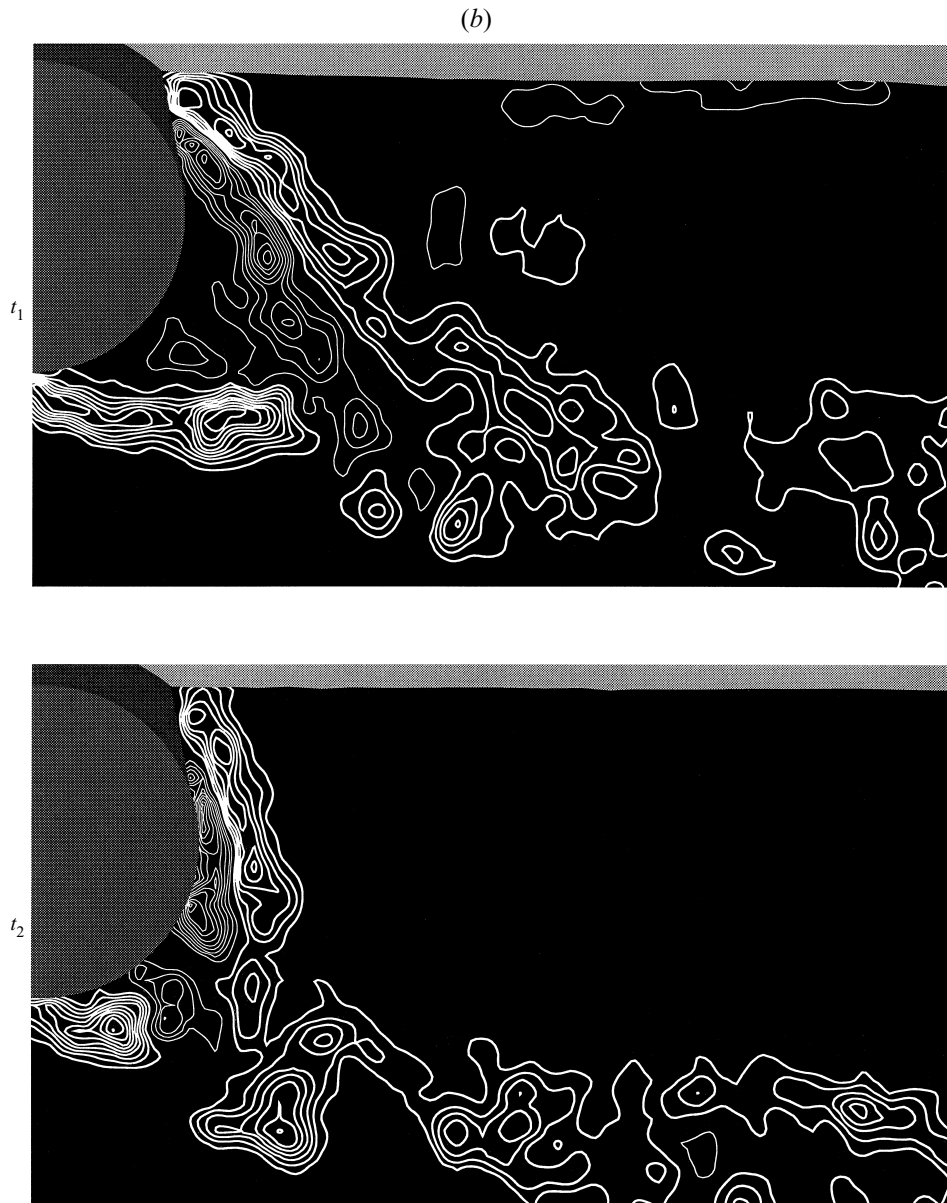


FIGURE 4. (a) Instantaneous velocity fields at two different instants of time t_1 and t_2 illustrating the variability in the wake state for the same Froude number $U/(gD)^{1/2} = 0.6$ and depth of the cylinder $h^* = h/D = 0.31$. The corresponding value of $U/(gh)^{1/2} = 1.08$. For these conditions, the jet-like structure flips between the two states shown. (b) Instantaneous vorticity fields matching the velocity fields in (a). Minimum and incremental vorticity contour levels are respectively $|\omega_{min}| = 20 \text{ s}^{-1}$ and $\Delta\omega = 20 \text{ s}^{-1}$.

4. Instability of wake states

For certain ranges of flow parameters and depths of submergence of the cylinder, two possible states of the wake can occur. Each of these states was metastable; the flow pattern drifted or flipped between the two states. In other words, a self-excited oscillation occurred at a very low, irregular frequency, typically one to two orders of

(a)

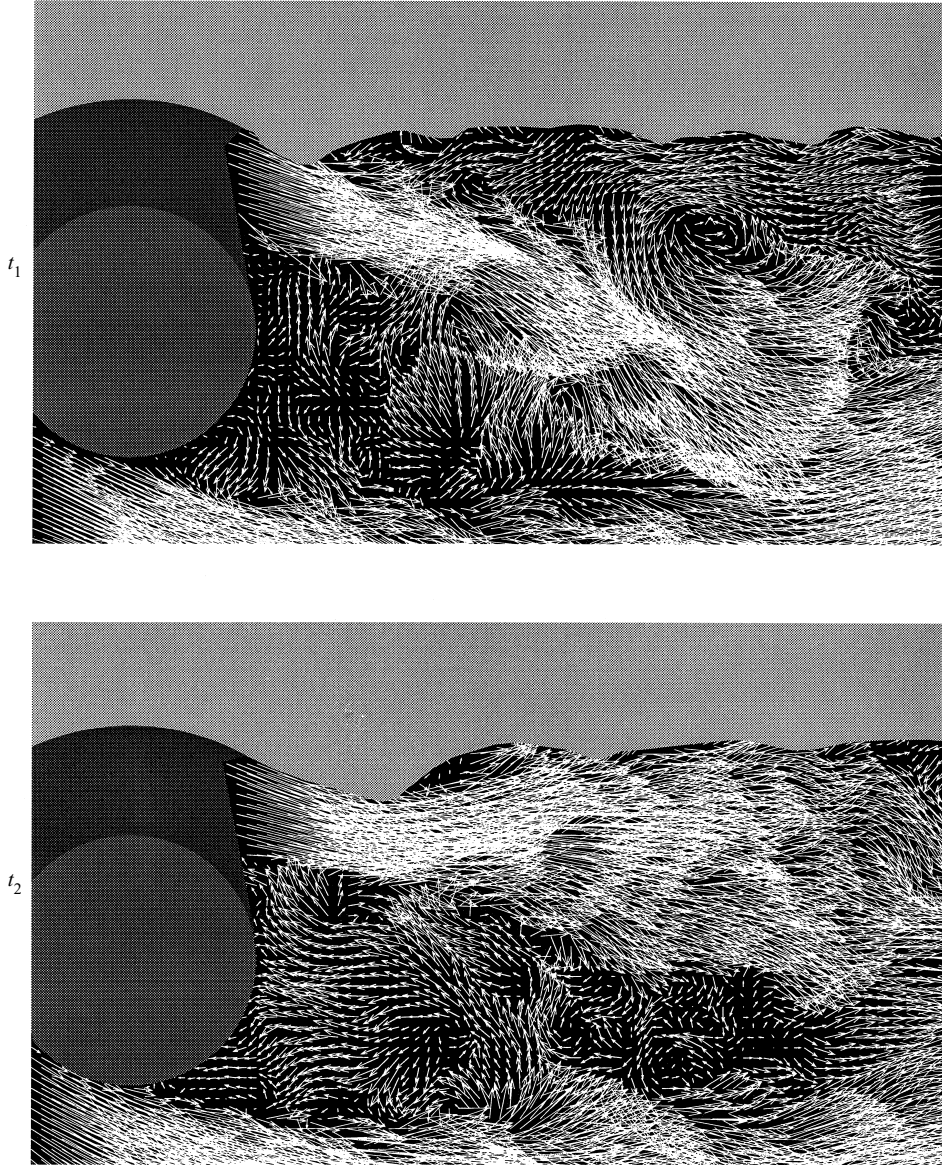


FIGURE 5(a). For caption see facing page.

magnitude lower than the Kármán frequency of vortex formation from the fully submerged cylinder. In view of the fact that these transformations between two distinct states are not periodic, it is not appropriate to define a universal dimensionless frequency.

4.1. *Oscillation adjacent to the base of cylinder*

Figures 4(a) and (b) show the case of self-excited oscillation between two states where the jet is detached from, and nearly attached to, the base of the cylinder. These two instants are indicated as t_1 and t_2 . In order for the detached jet to remain in equilibrium, a delicate mass balance is maintained between the flow entrained by the separated

(b)

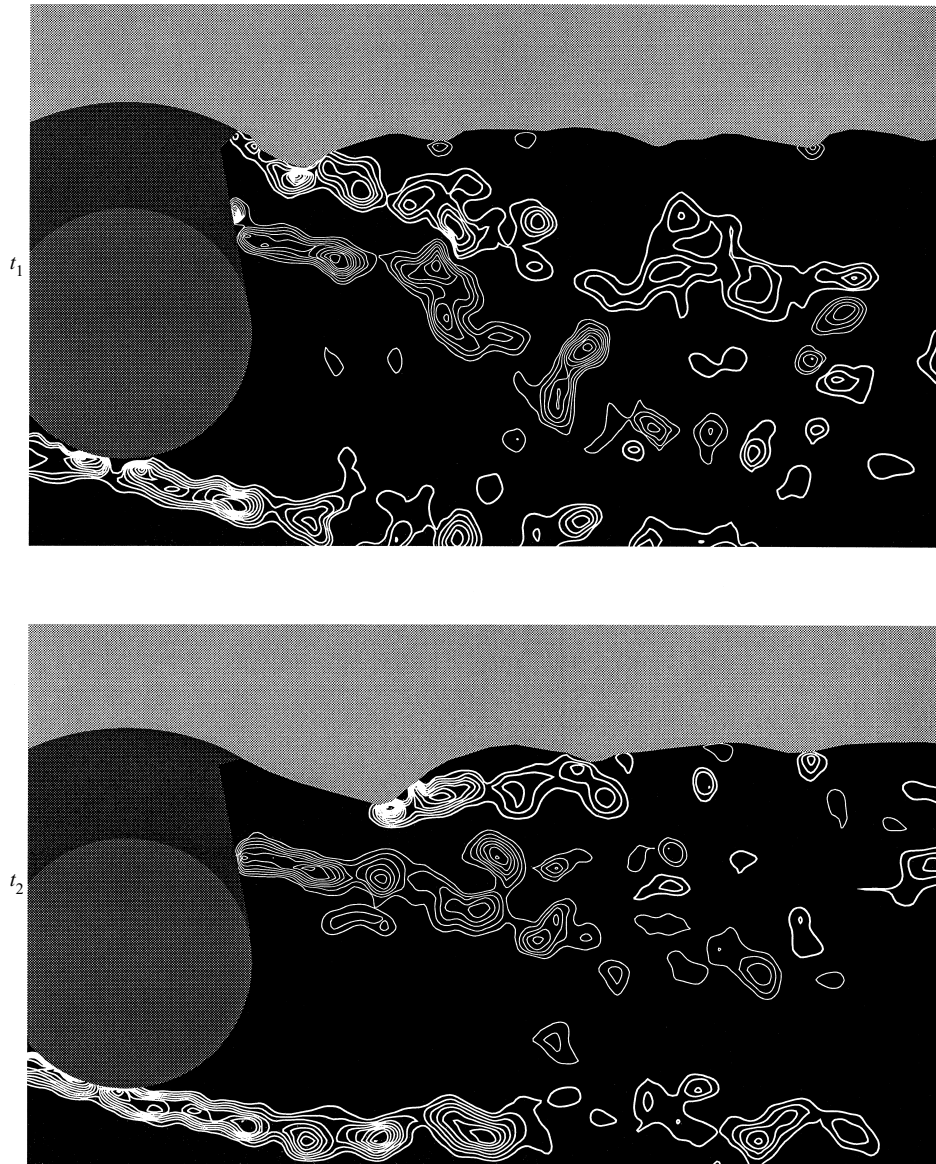


FIGURE 5. As figure 4 but for depth of cylinder $h^* = h/D = 0.59$. The corresponding value of $U/(gh)^{1/2} = 0.78$. For these conditions, the flow flips between the two states. In (b) minimum and incremental vorticity contour levels are respectively $|\omega_{min}| = 40 \text{ s}^{-1}$ and $\Delta\omega = 20 \text{ s}^{-1}$.

negative (thin lines) vorticity layer from the top surface of the cylinder and the flow deflected back to the base region when the jet merges with the vorticity layer from the bottom surface of the cylinder. In fact, close inspection of the image of the velocity field at t_1 in figure 4(a) shows a large-scale swirl pattern, and a small-scale one of opposite sense immediately beneath it. The large-scale pattern is of immediate interest. Its bottom portion represents the deflected flow towards the base and the top portion indicates the flow entrained to the negative vorticity layer of the jet. When insufficient

entrained flow is supplied, the jet will be deflected towards the base of the cylinder until a new balance between the entrained and deflected flow is attained. On the opposite (right-hand) side of the jet, a large-scale swirl pattern of velocity vectors is evident. We see therefore that the detached jet at instant t_1 is accompanied by a number of vortical patterns, whose delicate balance allows satisfaction of the entrainment demands on either side of the jet. When this entrainment balance is disturbed, the jet moves to the nearly attached state indicated at time t_2 in figure 4. This deflection towards the base of the cylinder is aided by onset of the well-known Coanda effect, whereby a jet tends to remain attached along the surface of a cylinder (Newman 1961). In this case, the large-scale counter-swirl pattern on the right-hand side of the jet has moved downward and to a location close to the cylinder. This state t_2 therefore represents a collapse of the delicately balanced swirl (vortical) pattern between the jet and the base of the cylinder shown at t_1 .

4.2. Oscillation adjacent to the free surface

Another type of self-excited oscillation involves two different states of the wake, designated as t_1 and t_2 in figures 5(a) and 5(b). The value of the Froude number, $Fr = 0.6$, is sufficiently high that distortion of the free surface plays a role. At t_1 , the large downslope of the free surface near the cylinder is associated with separation at the first trough. This positive (thick line) vorticity layer formed from the free surface eventually gives rise to a large-scale vortex immediately beneath the surface, suggested by the swirl pattern of velocity vectors in figure 5(a) and the corresponding region of vorticity in figure 5(b). In addition, an upstream flow occurs along the free surface. This counterflow, which has a relatively large magnitude, generally gives rise to concentrations of negative (thin lines) vorticity near/at the troughs of the free surface. The location and form of these concentrations are in accord with those occurring at small-amplitude depressions of the surface in the simulation of Dimas & Triantafyllou (1994).

The positive (thick flow) vorticity layer, which is separated from the free surface, forms a jet in conjunction with the negative (thin lines) layer from the surface of the cylinder. Concentrations of positive and negative vorticity on either side of the jet tend to be in phase, corresponding to a varicose or symmetrical mode of instability of the jet, in analogy with the well-known modes occurring in forced planar and axisymmetric jets (Ho & Huerre 1984).

As indicated in the velocity and vorticity images at t_2 , the jet eventually deflects upward, such that it is generally attached to the free surface. In this case, the downslope of the free surface at the location of the first trough is much milder than for the state at t_1 . The steepness of this first trough is, however, sufficient to induce local flow separation, giving rise to a mixing layer, which eventually attaches to the second trough of the free surface. This process exhibits the central features of a spilling breaker occurring in the absence of a cylinder, as described by Lin & Rockwell (1994, 1995).

The self-excited oscillation of figure 5 therefore exhibits two principal features, one associated with the free-surface distortion and vorticity generation from it, evident at both t_1 and t_2 , and the other with large-scale vortical motion between the free surface and the deflected jet, occurring at t_1 . The free-surface distortion is accompanied by localized wave breaking, involving mixing-layer formation beneath the first crest of the free-surface wave at t_2 . As the trough corresponding to the onset of breaking moves upstream, the downslope of the free surface ahead of the trough increases and the localized wave breaking is transformed to a fully separated vorticity layer from the free surface at t_1 . Then, agglomeration of vorticity in the separated vorticity layer gives rise

to the large-scale vortex between the free-surface and the detached jet. In turn, this large-scale vortex upstream is associated with (counter) flow along the surface, which satisfies the entrainment demands of the separated vorticity layer. These features of the metastable states at t_1 and t_2 , and the transformation between them, have several elements in common with the system described by Sheridan *et al.* (1995).

5. Wake states: effect of Froude number

In order to further examine the effects of free-surface wave motion on the states of the wake, the depth of submergence of the cylinder was maintained constant, and the free-stream velocity altered to generate a succession of free-surface distortions. Figures 6(a) and 6(b) show the wake structure corresponding to the lower range of Froude number. At $Fr = 0.22$, the jet velocity beneath the free surface is below the critical value for which wave motion occurs. Moreover comparison of the velocity and vorticity distributions shows that no large-scale Kármán vortices are formed within the field of view. The presence of the free surface clearly inhibits onset of the Kármán instability, yet allows small-scale Kelvin–Helmholtz (K–H) instabilities to occur, evident in the small-scale swirl patterns of velocity vectors and the corresponding vorticity contours. At $Fr = 0.35$, a free-surface wave occurs with a relatively long and irregular wavelength. In this case, the negative (thin lines) layer of vorticity formed from the top surface of the cylinder exhibits small-scale K–H concentrations of vorticity. This layer eventually attaches to the second, broad trough of the free-surface wave. Regarding the flow in the central portion of the wake, relatively larger counterflow exists in regions well upstream, extending nearly to the base of the cylinder. This counterflow contrasts with the relatively quiescent region adjacent to the base of the cylinder at $Fr = 0.22$. At a higher value of $Fr = 0.47$, small-scale localized wavebreaking occurs. It is represented by the positive (thick lines) layer of vorticity from the first trough of the wave pattern. Simultaneously, the negative (thin lines) vorticity layer from the surface of the cylinder now attaches to the second trough immediately downstream of the localized wave-breaking zone. This occurrence of small-scale wavebreaking results in loss of periodicity of the wave pattern evident at $Fr = 0.35$.

Over the higher range of Froude numbers, corresponding to the images of figures 7(a) and 7(b), the free surface at $Fr = 0.60$ again exhibits a nearly spatially periodic distortion of the free surface in the form of a stationary wave. Well-defined wave breaking is initiated at the first trough, and high values of vorticity occur in the mixing layer that is formed downstream of the trough. Downstream of this region of wave breaking, the amplitude of the free-surface distortion diminishes substantially. Its spatial periodicity is retained, however, and well-defined concentrations of positive vorticity occur at the troughs. The negative (thin lines) vorticity layer formed from the upper surface of the cylinder reattaches to the second trough of the surface wave, then detaches from the surface. At $Fr = 0.72$, the free surface takes on an essentially undistorted form, owing to complete separation of the vorticity layer from the free surface. The small-scale concentrations of vorticity formed both in the vorticity layer from the free surface and in the layer from the upper surface of the cylinder exhibit pronounced K–H concentrations of vorticity, which tend to occur in pairs. Finally, at the highest value of the Froude number, $Fr = 0.97$, the elevation of the free surface is substantially lower, and the onset of separation from it, leading to the positive vorticity layer, has moved downstream away from the base of the cylinder. Again, the correspondence between small-scale K–H concentrations of vorticity between the

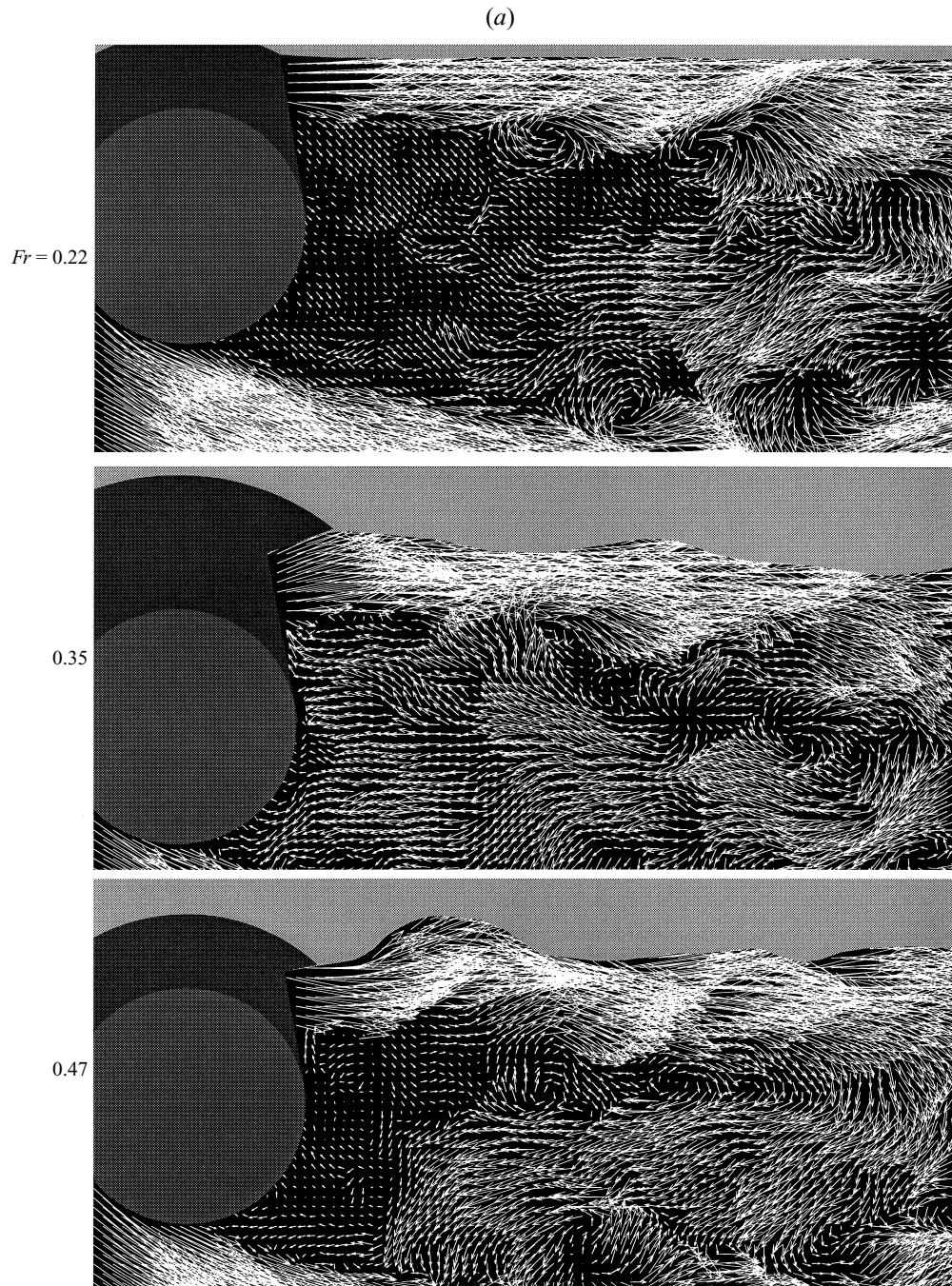


FIGURE 6(a). For caption see facing page.

layers from the free surface and the top surface of the cylinder is remarkable. This correspondence indicates that the instabilities in both of these layers evolve in a highly coupled fashion, with strong communication between the fluctuations in both layers. At both $Fr = 0.72$ and 0.97 , the vorticity in the right-hand half of the images is

(b)

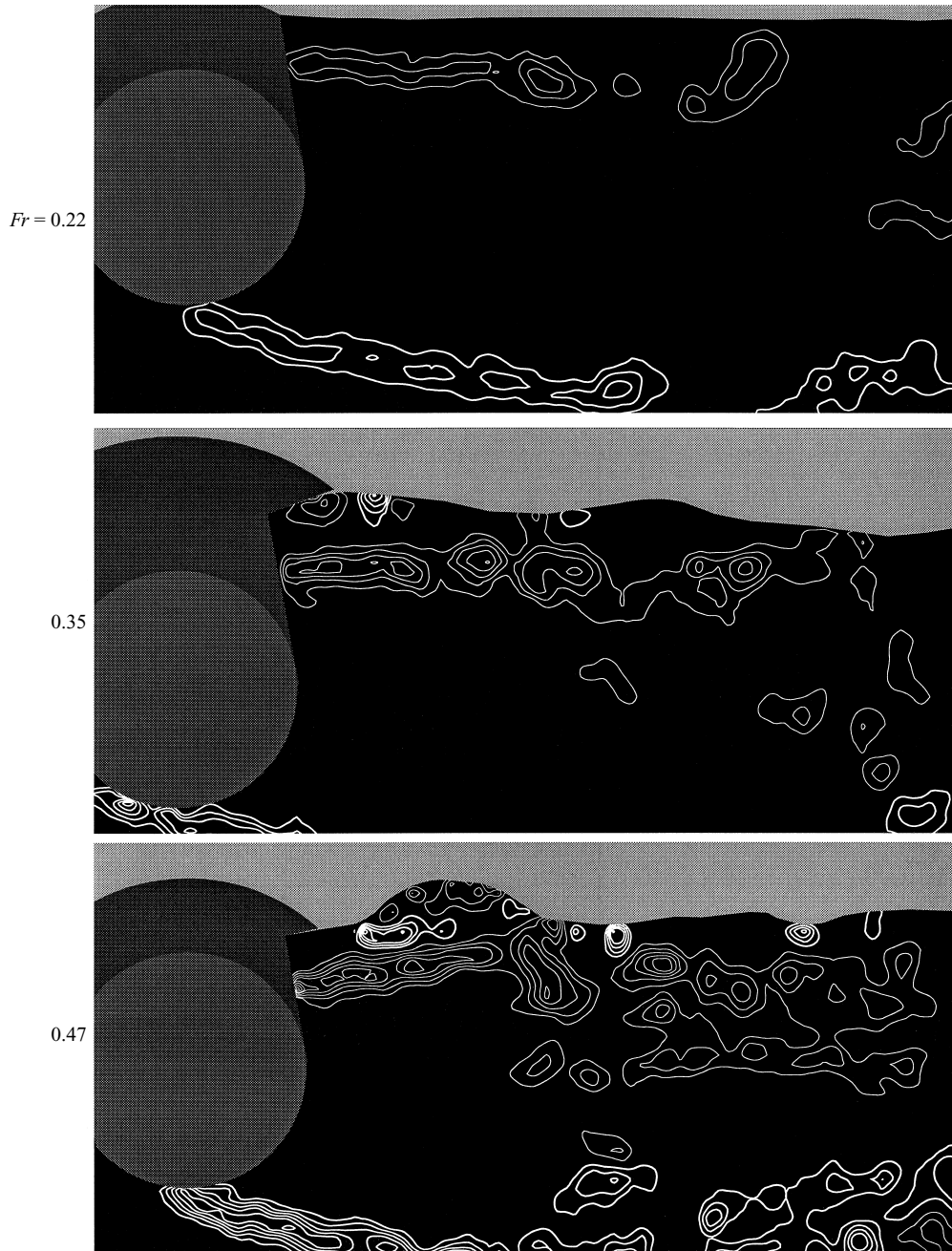


FIGURE 6. Instantaneous velocity fields and free-surface shapes obtained by varying the Froude number over a range of relatively low values $0.22 \leq U/(gD)^{1/2} \leq 0.47$ at a constant depth of the cylinders $h^* = h/D = 0.40$. Corresponding values of $U/(gh)^{1/2} = 0.34, 0.55, 0.74$. (b) Instantaneous vorticity fields corresponding to (a). Minimum and incremental contour levels are respectively $|\omega_{min}| = 20 \text{ s}^{-1}$ and $\Delta\omega = 20 \text{ s}^{-1}$.

(a)

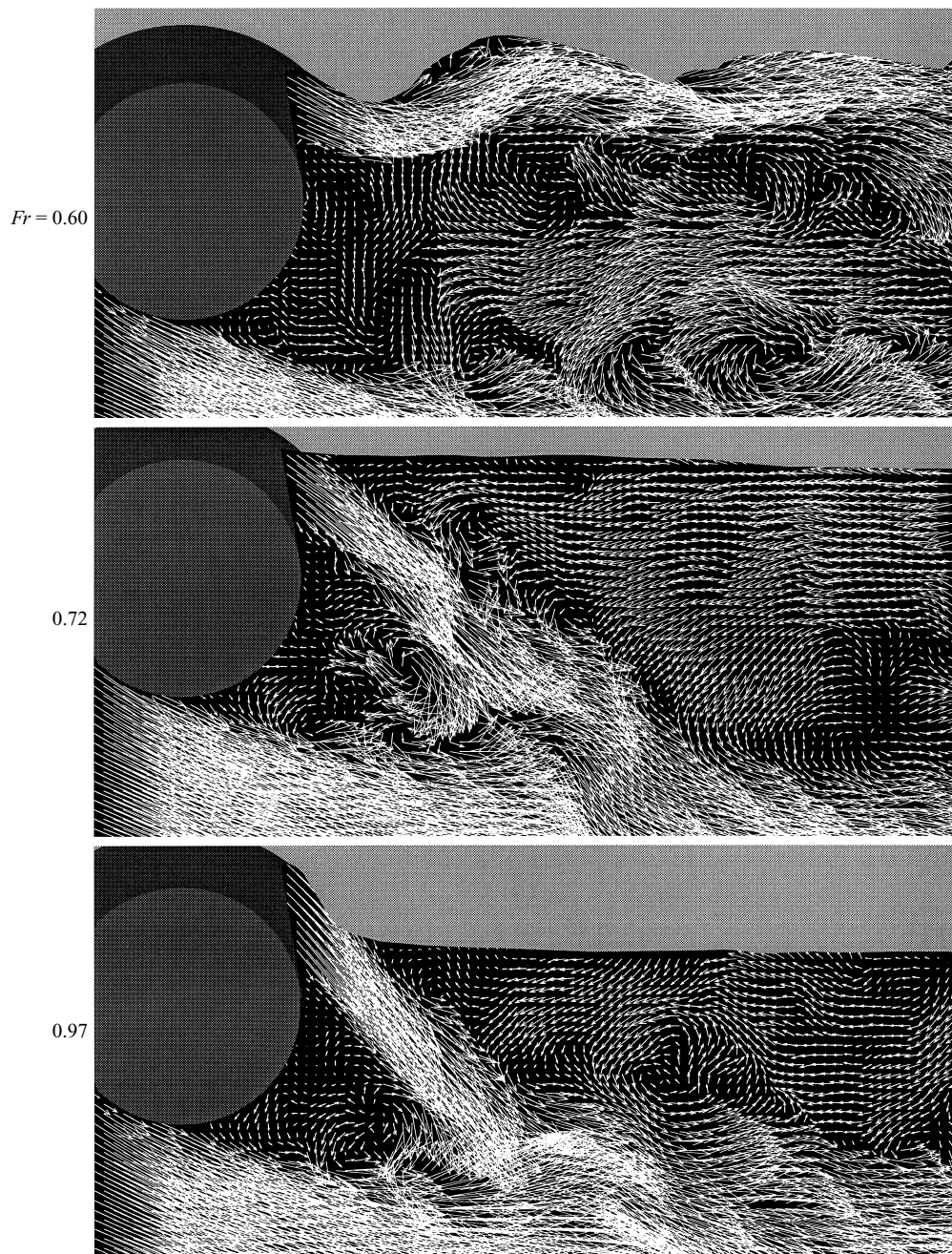


FIGURE 7(a). For caption see facing page.

dominated by positive vorticity; this sign of the vorticity is in accord with the slope of the velocity distribution across the mixing layer in that region.

It is possible for the wake states to take on generally similar forms at extreme combinations of Fr and h^* , in the absence of distortion of the free surface. The images

(b)

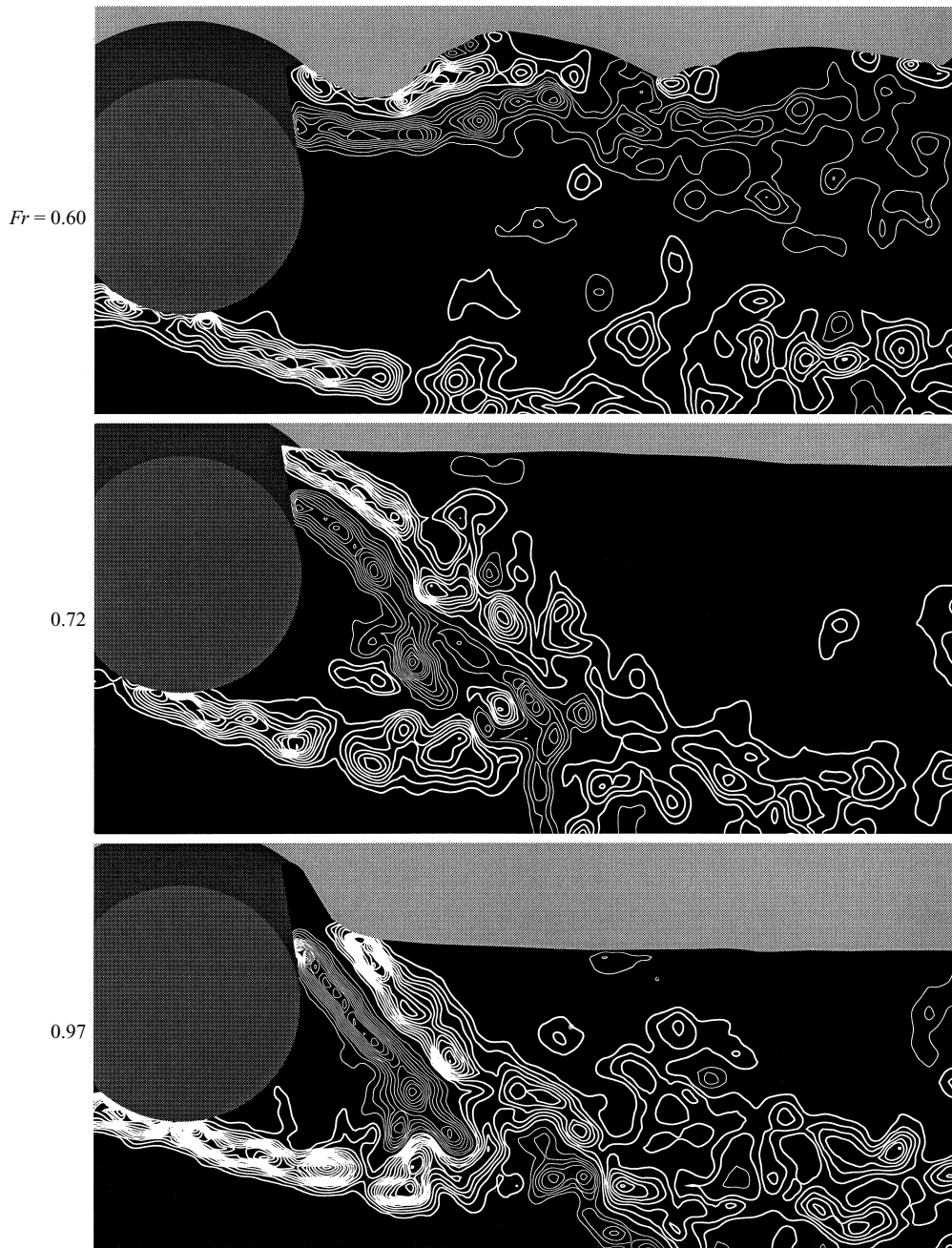


FIGURE 7. As figure 6 but varying the Froude number Fr over a range of relatively high values $0.6 \leq U/(gD)^{1/2} \leq 0.97$. Corresponding values of $U/(gh)^{1/2} = 0.95, 1.14, 1.53$.

of figures 8 and 9 illustrate this point. In figure 8, at the extreme values of $Fr = 0.47$ and 0.72 , similar states could be generated by adjusting the depth of submergence of the cylinder to values of $h^* = 0.28$ and 0.20 , respectively. For both of these cases, the jet tends to remain attached along the base of the cylinder, and merge with the

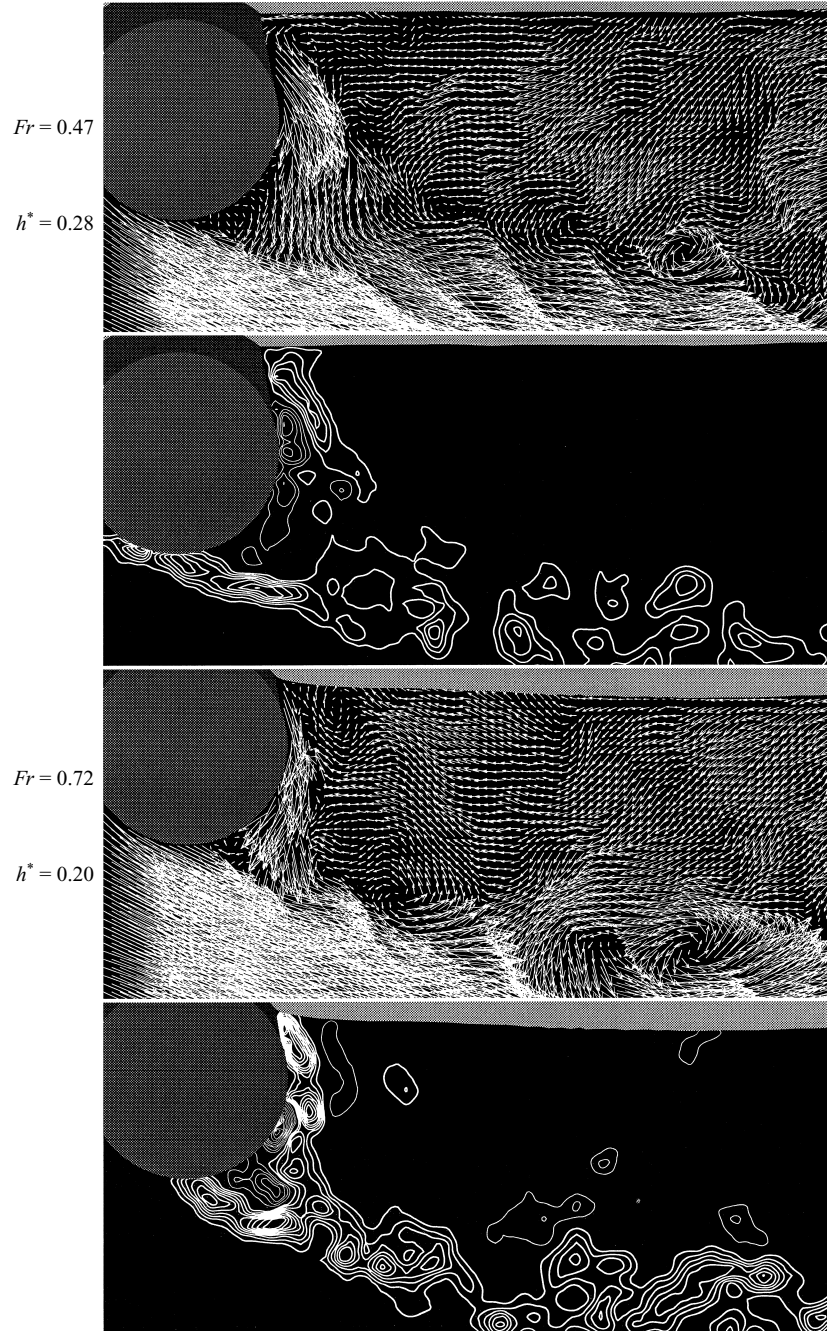


FIGURE 8. Velocity and vorticity fields showing the similarity between flow states that can occur for extreme values of Froude number $U/(gD)^{1/2}$ by properly adjusting the depth of the cylinder $h^* = h/D$. Corresponding values of $U/(gh)^{1/2} = 0.88$ and 1.60 . The jet-like flow tends to remain attached to the base of the cylinder and interacts with the shear layer formed from the lower surface of the cylinder. Minimum and incremental countour levels are respectively $|\omega_{min}| = 20 \text{ s}^{-1}$ and $\Delta\omega = 20 \text{ s}^{-1}$.

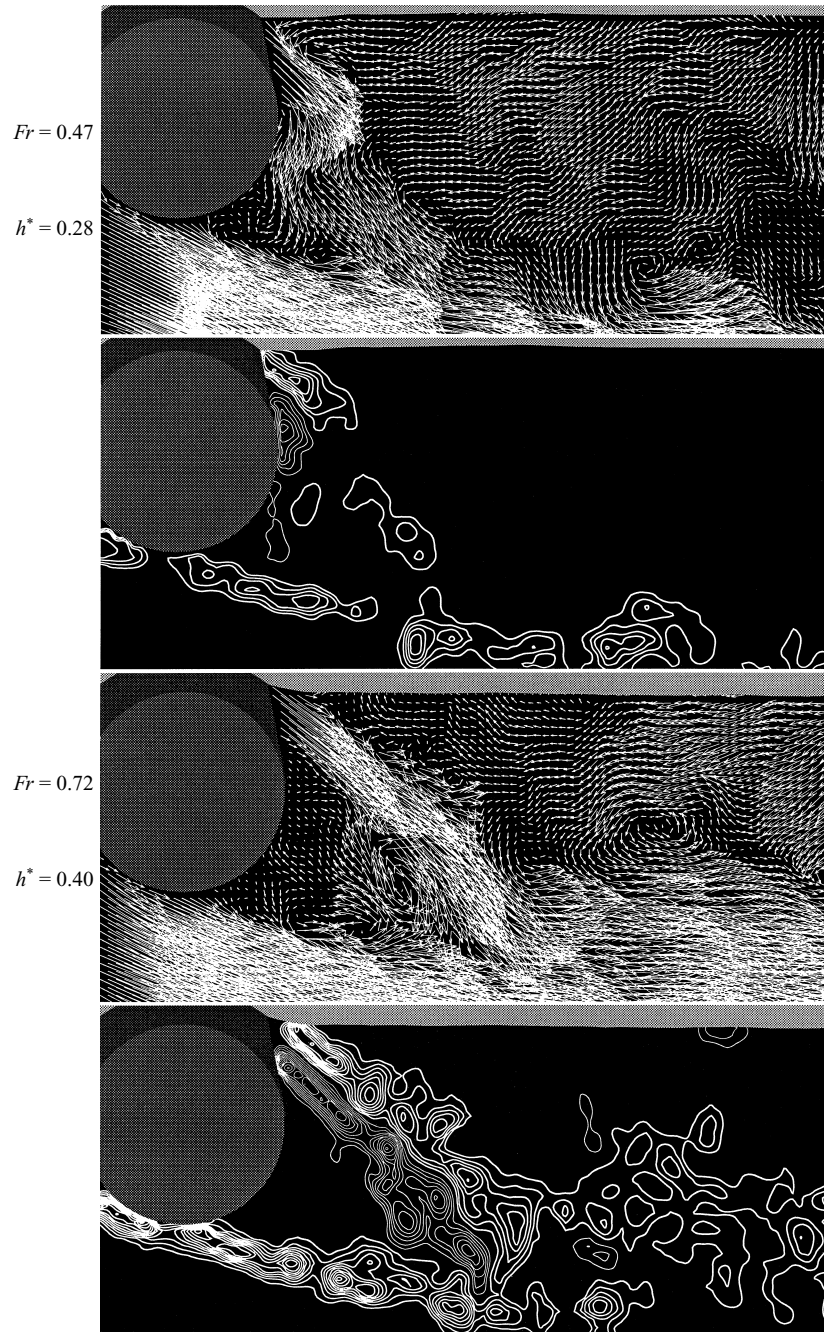


FIGURE 9. Instantaneous velocity and vorticity fields showing the similarity between the flow states that can occur for extreme values of Froude number $U/(gD)^{1/2}$ by properly adjusting the depth of the cylinder $h^* = h/D$. Corresponding values of $U/(gh)^{1/2} = 0.88$ and 1.14 . The jet-like flow is detached from the cylinder and interacts with the separating shear layer well downstream of the cylinder. Minimum and incremental contour levels are respectively $|\omega_{min}| = 20 \text{ s}^{-1}$ and $\Delta\omega = 20 \text{ s}^{-1}$.

separated mixing-layer from the bottom surface of the cylinder in a very similar fashion to that of the intermediate value of $Fr = 0.6$ and $h^* = 0.24$ illustrated in figures 2(a) and 2(b). The key to generating these similar states is to preclude the tendency of the jet to become attached to the free surface. At each of the foregoing combinations of Fr and h^* , the Coanda effect preserves the jet attachment along the base of the cylinder. Particularly remarkable is the maintenance of this state at the relatively high value of $Fr = 0.72$, provided the depth of submergence is kept small at $h^* = 0.20$.

Approximate similarity of the wake states at the same two extreme values of $Fr = 0.47$ and 0.72 can also be attained, when the depth submergence of the cylinder is adjusted respectively to values of $h^* = 0.28$ and 0.40 . The overall form of this wake state, which involves a jet-like flow detached from the surface of the cylinder and merging with the mixing layer from the bottom of the cylinder at a location well downstream, has a remarkably similar form to that shown in figures 3(a) and 3(b). The particular combination of Fr and h^* giving rise to these states depends strongly on the conditions for which the jet detaches from the free surface. In turn, these conditions are a function of the particular type of wave pattern at the free surface preceding the onset of jet detachment (compare cases of $Fr = 0.60$ and 0.72 in figure 7). Depending upon whether the small-scale wave breaking occurs at the first trough (figures 5 and 7) or at the second trough (Sheridan *et al.* 1995), the combination of Fr and h^* yielding jet detachment will differ.

6. Free-surface distortion and wake states at large depths of cylinder

When the cylinder is located at relatively large depths beneath the free surface, the extent of the downslope region of the surface is much longer, that is, the steepness is milder than illustrated in the foregoing cases. Patterns of localized wave breaking and jet formation may be either similar to, or different from, those arising in the aforementioned systems of spatially periodic waves, depending on the degree of submergence of h^* . Well-defined wave breaking occurs at $h^* = 2.0$ in figure 10. It generates a separated layer having a high level of vorticity while remaining parallel to the free surface. A pronounced concentration of vorticity occurs at the location of abrupt change in curvature of the free surface, marking the onset of flow separation. In essence, these features are similar to those occurring in the spatially periodic wave systems of figures 5 and 7. A decrease in submergence to $h^* = 1.18$, however, generates sharp irregularities in the free surface. The first irregularity, taking the form of a sharp trough, generates high levels of vorticity, apparently in the absence of flow separation in that region. At the second, much milder trough, flow separation occurs and the thickness of the vorticity layer separating from the free surface increases substantially, eventually exhibiting a large patch of vorticity due to abrupt downward displacement of the separated vorticity layer. Finally, at $h^* = 0.79$, the free surface is relatively quiescent, and separation of the positive layer of vorticity from it occurs immediately downstream of the cylinder. For all values of h^* , indicated in figure 10, there is a substantial region of irrotational flow between the positive vorticity layer from the free surface and the negative one from the upper surface of the cylinder. This type of jet-like flow contrasts with the closely spaced and strongly coupled vorticity layers generated in the foregoing for much lower submergence of the cylinder, i.e. smaller h^* . As a consequence of the large extent of the irrotational region between the vorticity layers, the streamwise development of the concentrations of vorticity appears to occur independently in each layer, as suggested by the patterns of vorticity concentrations in the image at $h^* = 0.79$.

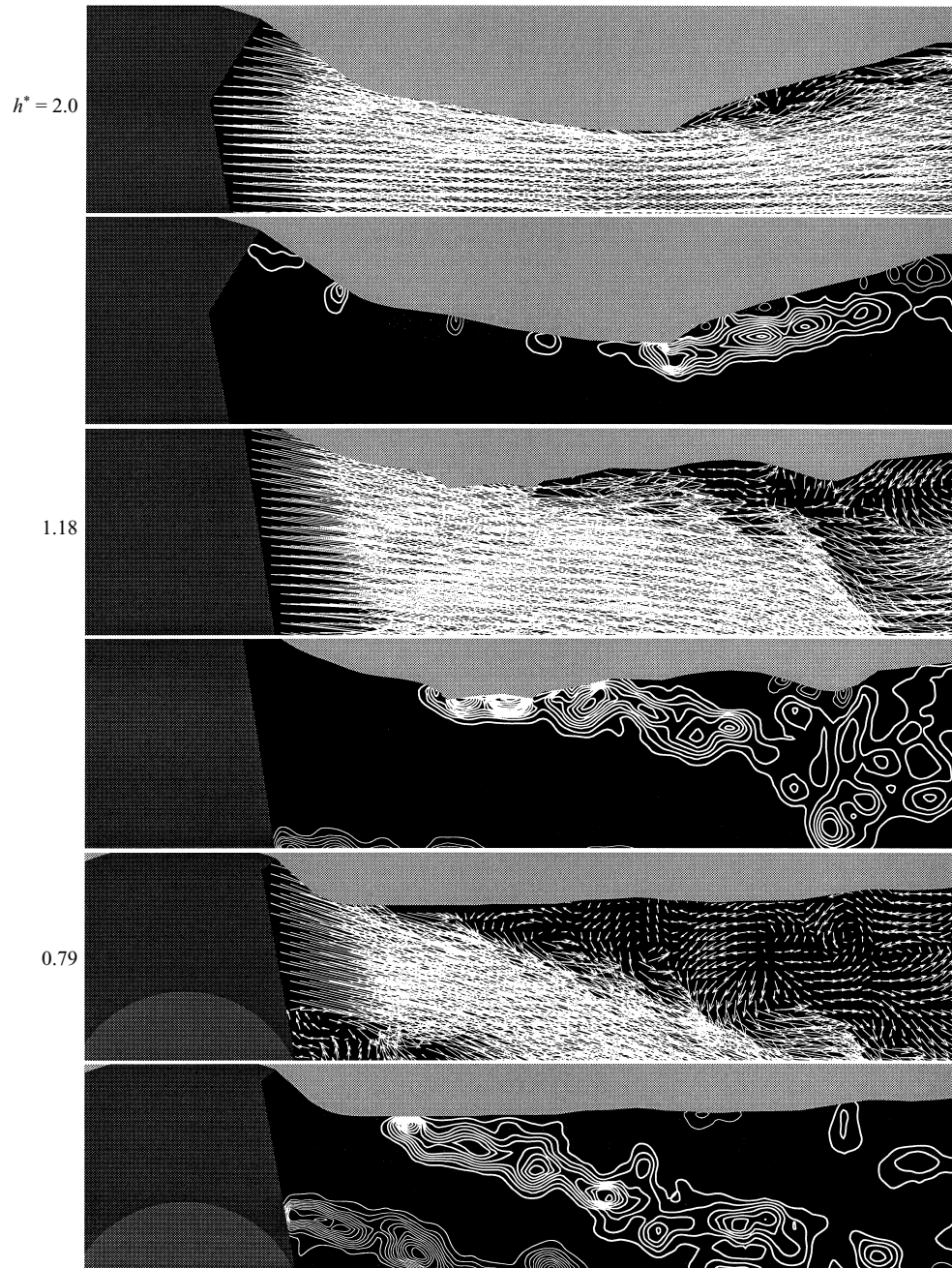


FIGURE 10. Instantaneous velocity and vorticity fields and corresponding shapes of the free surface generated at large depths of submergence of the cylinder $h^* = h/D$ for constant Froude number $U/(gD)^{1/2} = 0.72$. Corresponding values of $U/(gh)^{1/2} = 0.51, 0.66,$ and 0.86 . Minimum and incremental contour levels are respectively $|\omega_{min}| = 20 \text{ s}^{-1}$ and $\Delta\omega = 20 \text{ s}^{-1}$.

7. Vorticity flux from free-surface and surface of cylinder

The vorticity layers from the free surface and the upper surface of the cylinder play a central role in determining the structure of the near wake and the free-surface distortion. As illustrated, for example, in figures 7(a) and 7(b), irrespective of whether the jet-like flow remains nominally attached to the free surface or is deflected downward from it, there appears to be a strong interaction between these layers, and an assessment of the corresponding vorticity fluxes is in order. Reynolds & Carr (1985) describe the vorticity balance concept of shear flows and address the specific case of a free mixing layer. By analogy, it is possible to demonstrate, for the case of a laminar jet in free space, that the vorticity flux F has the same magnitude on either side of the jet. Let

$$F^+ = \int_0^{\infty} u\omega_z dy, \quad F^- = \int_{-\infty}^0 u\omega_z dy, \quad (1)$$

in which u is the local streamwise velocity, ω_z is the local spanwise vorticity and y is normal to the jet axis. Then

$$F^+ = F^- \quad (2)$$

at any section of the quasi-parallel jet. The jet-like flows shown in figure 7, however, do not satisfy this idealized case owing to two limitations. First of all, they are not unbounded, i.e. surrounded by free space; and secondly, the jets are not laminar, owing to amplification of the Kelvin–Helmholtz instability waves that induce spatial variations of instantaneous vorticity in each of the layers comprising the jet. However, the concentrations of vorticity appearing in the jet-like flows tend to be spatially periodic and it is useful to compare instantaneous vorticity fluxes at sections corresponding to maxima and minima of the vorticity distributions in the jet. Then, by constructing the spatial average over the streamwise extent of each of the jet-like flows, it will be possible to approximate the extent to which the vorticity fluxes on either side of the jet-like flow are, on average, satisfied.

First, consider the case corresponding to the jet that is nominally attached to the free surface, shown at $Fr = 0.60$ in figure 7(b). The region of interest beneath the free surface is defined by the schematic of figure 11(a). The coordinate s is along the instantaneous streamline between the positive and negative regions of vorticity, and the origin $s = 0$ is at the trough of the small-scale wave breaking beneath the free surface. Coordinate y is the local normal to this streamline. Lines A – E are normal to s and pass approximately through maxima and minima of instantaneous concentrations of vorticity. The layer of negative vorticity from the surface of the cylinder originates well upstream of the $s = 0$ location; substantial flux of negative vorticity therefore exists beneath the trough of the free surface. In contrast, there is only very low-level positive vorticity, arising from the free-surface curvature upstream of $s = 0$. Just downstream of the trough, at section B , a concentration of positive vorticity abruptly appears; it occurs in harmony with a corresponding concentration of negative vorticity. Further downstream, sections C , D and E correspond, respectively, to local minima, maxima, then minima of the vorticity distributions. We first consider the velocity profiles at sections A – D , indicated in the left-hand column of figure 11(a). They are asymmetric at all locations, with particularly high gradients occurring in the region of positive vorticity corresponding to $y/D > 0$. Despite this asymmetry, the corresponding velocity fluxes F^+ and F^- indicated in the right-hand column of figure 11(a) appear to be nearly balanced at sections B and D , which pass through the vorticity maxima. In summary, the localized wave-breaking process shown in figure 11(a), which occurs in

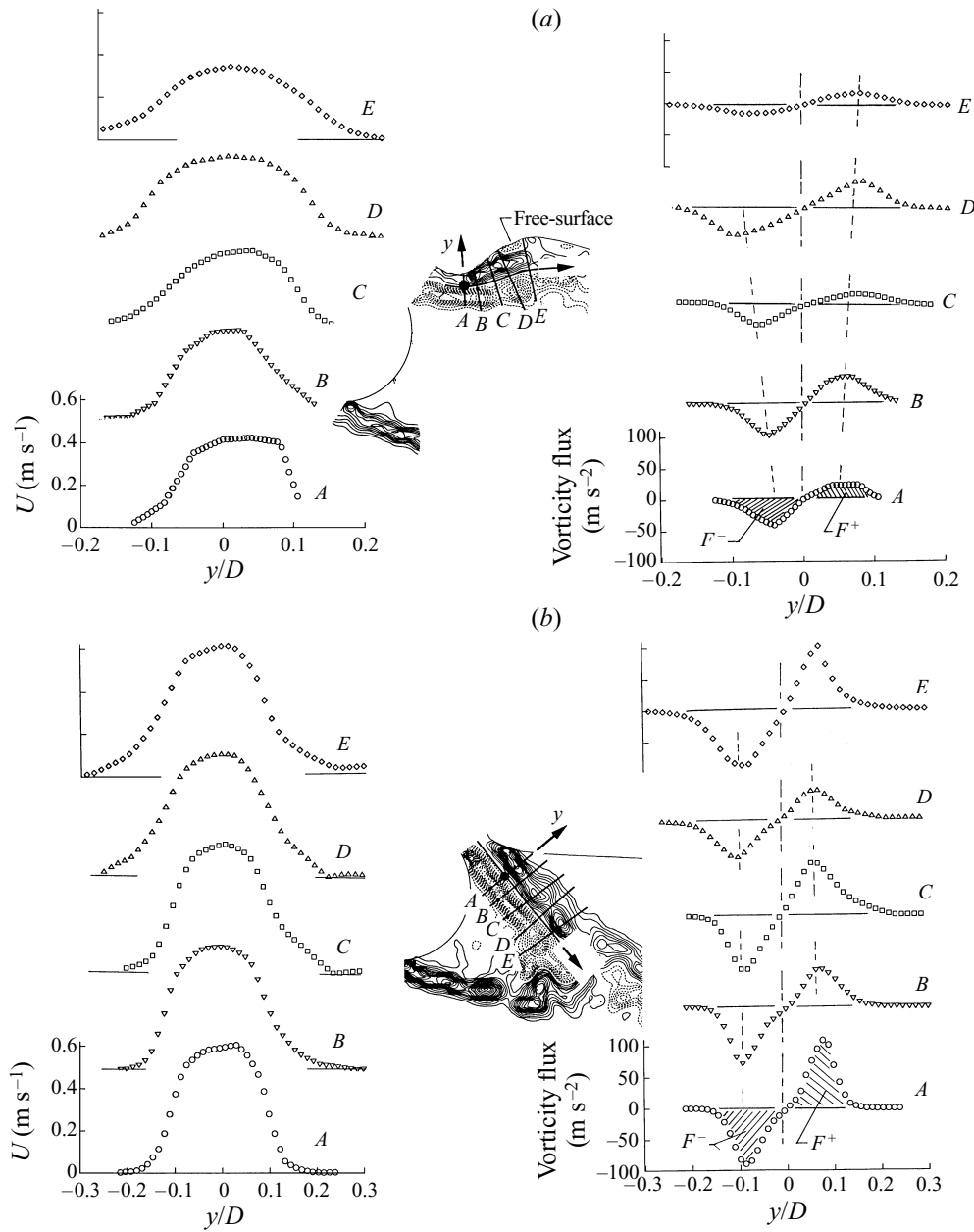


FIGURE 11. Profiles of instantaneous velocity and vorticity flux $u\omega_z$, in which u is axial velocity and ω_z is spanwise vorticity, at successive cross-sections designated as A–E. Data correspond to figure 7 (a) $Fr = 0.60$, (b) $Fr = 0.97$.

the presence of a pre-existing layer of vorticity from the cylinder, very rapidly generates a balanced, jet-like system of vorticity flux; this process is an important prelude to detachment of the jet from the free surface.

The case of the fully-deflected jet from the free surface is represented in the schematic of figure 11(b); it corresponds $Fr = 0.97$ in figure 7(b). The layer of negative vorticity from the cylinder pre-exists at the streamwise location corresponding to separation

Section	Jet-like flow at onset of wave breaking ¹		Initially deflected jet from free surface ²		Fully deflected jet from free surface ³	
	F^+	F^-	F^+	F^-	F^+	F^-
<i>A</i>	0.043	-0.06	0.072	-0.088 [ω_{max}]	0.185	-0.173 [ω_{max}]
<i>B</i>	0.079	-0.081 [ω_{max}]	0.098	-0.086	0.137	-0.175
<i>C</i>	0.063	-0.037	0.084	-0.078 [ω_{max}]	0.225	-0.180 [ω_{max}]
<i>D</i>	0.082	-0.122 [ω_{max}]	0.094	-0.082	0.115	-0.153
<i>E</i>	0.041	-0.045	0.052	-0.136 [ω_{max}]	0.200	-0.273 [ω_{max}]
F_{avg}	0.06	-0.07 m ² s ⁻²	0.08	0.09 m ² s ⁻²	0.17	-0.19 m ² s ⁻²
$\left[\frac{1}{2}U_j^2\right]_A$		0.09 m ² s ⁻²		0.09 m ² s ⁻²		0.18 m ² s ⁻²
$\left[\frac{1}{2}U_j^2\right]_{avg}$		0.08 m ² s ⁻²		0.09 m ² s ⁻²		0.18 m ² s ⁻²

¹ Corresponds to figure 7 ($Fr = 0.60$) and figure 11(a).

² Corresponds to figure 7 ($Fr = 0.72$)

³ Corresponds to figure 7 ($Fr = 0.97$) and figure 11(b).

TABLE 1. Instantaneous vorticity fluxes

from the free surface; this pre-existence of the negative layer is analogous to that occurring in figure 11(a). Both the negative and positive layers exhibit high levels of vorticity. The maxima of the vorticity concentrations are, however, more pronounced in the positive layer from the free surface. Eventually, at section *E*, the concentrations of vorticity in both layers have approximately the same order. Considering first the velocity profiles in the left-hand column of figure 11(b), they exhibit substantial asymmetry, with the largest velocity gradients occurring in the layer of negative vorticity of the cylinder, i.e. for $y/D < 0$. However, as shown in the corresponding plots of vorticity flux in the right column of figure 11(b), the instantaneous vorticity fluxes F^+ and F^- at sections *A* and *C* appear to be balanced. It therefore appears that balance of vorticity is rapidly achieved immediately upon separation from the free surface.

A quantitative comparison of the instantaneous vorticity fluxes at sections *A* to *E* is given in table 1, not only for the cases illustrated in figures 11(a) and 11(b), but also for the intermediate case of the initially deflected jet from the free surface, corresponding to $Fr = 0.72$ in figure 7(b). Local maxima of the vorticity concentrations are indicated by ω_{max} . The averaged vorticity flux F_{avg} corresponds to the average of the instantaneous values at sections *A* to *E*. For each of the three jet-like flows, the averages of fluxes F^+ and F^- are nearly equal. The values of F_{avg} for the initially deflected jet ($Fr = 0.72$) are only slightly larger than those for the jet-like flow at the onset of wave breaking ($Fr = 0.60$) in figure 7(b). In contrast, for the fully deflected jet ($Fr = 0.97$), the magnitudes of the fluxes are nearly doubled. It can be seen by comparing the radii of curvature of the free surfaces at the onset of separation in figure 7(b) that the radius of curvature is substantially smaller at $Fr = 0.97$ relative to that at 0.72, suggesting a relation between the curvature of, and the flux through, the free-surface.

For the case of a laminar, quasi-parallel jet in the free space, if there exists a small irrotational region along the centre of the jet having velocity U_j , and the vorticity distribution is approximated as linear, then vorticity balance concepts show that the

magnitude of the flux $F^+ = F^- = U_j^2/2$. This term was evaluated at section A , corresponding to the subscript A in table 1; in addition, it was evaluated using the average velocity at sections A to E , designated in table 1 by the subscript *avg*. Both approaches give values of $U_j^2/2$ that approximate remarkably well the averages of fluxes F^+ and F^- .

The approximate equality of the vorticity fluxes F^+ and F^- has important implications for their origin. The flux from the surface of the cylinder is due to the pressure gradient $\partial p/\partial s$ along its surface. Although $\partial p/\partial s$ is finite along the entire extent of the curved surface of the cylinder, its value is large immediately preceding the onset of separation. Corresponding, the flux from the free surface can be represented as $U_s dU_s/ds$, in which U_s is the tangential velocity at the free surface. Likewise, this term has its largest value immediately preceding separation from the free surface. Now the curvatures of the surface of the cylinder and the free surface will dictate the values of $\partial p/\partial s$ and $U_s dU_s/ds$ at separation. Once the radius of the curvature of the cylinder is fixed, the curvature of the free surface will adjust itself to provide a flux of vorticity into the jet-like flow, which matches that from the surface of the cylinder.

8. Overview of free-surface wave patterns and vorticity layers

Irrespective of whether one considers variations in depth of the submergence h^* of the cylinder or Froude number Fr , the basic wake states that dictate free-surface distortion are: jet attachment to the free surface; and separation from it. When the jet is generally attached to the free surface, and the velocity beneath it exceeds a critical value, the amplitude of the free-surface distortion, i.e. wave motion, is unusually large. This is hypothesized to be due to a resonance effect, involving coupling between the surface distortion and the large-scale region of flow separation in the wake of the cylinders. The wavelength of the surface waves for these resonant states (figure 3, at $h^* = 0.75$; figure 5, at t_2 ; figure 7, at $Fr = 0.60$) can be approximated[†] by considering the wave speed c of an irrotational free-surface wave, accounting for both gravity g and surface tension T effects (Lighthill 1978):

$$c = \left[\frac{g}{k} + \frac{T}{\rho k} \right]^{1/2}. \quad (3)$$

To apply this relation to the present case, we interpret the wave train behind the cylinder moving at constant speed U (the wave with phase speed relative to still water opposite to the flow speed), yielding substitution of the U for c . Moreover, the wave pattern is standing, or stationary, in accord with the concept described by Lighthill (1978). For all three cases described in the foregoing, $Fr = 0.6$ and $U = 29.7 \text{ cm s}^{-1}$. Letting $g = 981 \text{ cm s}^{-2}$, $T/\rho = 72 \text{ cm}^3 \text{ s}^{-2}$, the wavelength $\lambda = 2\pi/k = 5.08 \text{ cm}$. The corresponding value of $\lambda/D = 2.0$ compares with those measured from figures 3, 5 and 7: $\lambda/D = 2.0, 0.96, \text{ and } 1.23$. These variations of λ/D are no doubt influenced by the magnitude of the jet velocity, which varies with submergence h^* , and is not accounted for in the foregoing considerations.

For the two smallest values of $\lambda/D = 0.96$ and 1.23 in figures 5 and 7, localized wave breaking occurs at the first trough of the wave. This localized breaking leads to formation of positive vorticity concentrations. This separated vorticity layer occurring beneath the crest of the free surface of the small-scale breaking wave in figures 5 and

[†] This approach was initially suggested by a referee of the manuscript of Sheridan, Lin & Rockwell (1995).

7 is the precursor of large-scale separation of the vorticity layer from the free surface. It arises from two simultaneous events: upstream movement of the trough from which separation occurs; and increased steepness of the free surface immediately preceding the trough. The maximum levels of vorticity observed for this fully separated vorticity layer are relatively high.

The important consequence of this fully separated vorticity layer from the free surface, as far as the free-surface signatures is concerned, is to produce a nearly quiescent, i.e. flat, surface. In certain situations, however, counter (reverse) flow occurs in the upstream direction beneath the surface. The magnitude of this counterflow is sufficient to induce small-scale troughs in the mildly distorted surface, as shown in figure 5 at instant t_1 . These small-amplitude, but steep, depressions are generally accompanied by localized concentrations of negative vorticity, much in the spirit of small-scale pinching of the surface due to an instability arising from a mean shear flow along the surface, as simulated by Dimas & Triantafyllou (1994).

The state of the fully separated vorticity layer from the free surface exhibits an overall form that is distinctly different from that occurring beneath a free-surface breaker in absence of a cylinder (Lin & Rockwell 1994, 1995). In that case, there are irregular undulations of the free surface in the region just above the vorticity layer. In the present case, however, there is a large angle of departure of the vorticity layer from the free surface, due to the presence of the cylinder. The cylinder strongly influences the curvature of the free surface above it, and thereby the location where separation occurs from the free surface. An issue not completely resolved is definition of the possible states of the jet for a wide parametric range of depth of submergence h^* and Froude number Fr . The degree of co-dependence of these parameters needs to be established in conjunction with, for example, scaling of the jet momentum with Fr .

Irrespective of whether one considers formation of the separated vorticity layer during the initial stage of small-scale wave breaking, or the occurrence of large-scale flow separation from the free surface corresponding to detachment of the jet from the surface, crucial features are common to both. Curvature of the free surface is essential for rapid onset of separation from it. In turn, the flow pattern immediately preceding the occurrence of separation undergoes very rapid distortion, involving a precipitous drop in the magnitude of the velocity along the surface. This process gives rise to substantial flux of vorticity, i.e. vorticity transport, into the region of fluid downstream of separation. In fact, as shown by Lin & Rockwell (1994, 1995), the onset of wave breaking from a region of the free surface having small curvature occurs in an analogous fashion. It involves a very abrupt, nearly discontinuous, decrease in streamwise velocity as the location of separation is approached. This process leads to the onset of high levels of vorticity.

The unsteady development of the fully separated vorticity layer from the free surface may occur relatively independently of the neighbouring layer of opposite vorticity generated from the top surface of the cylinder; this scenario occurs when the cylinder is at relatively large depths of submergence and a substantial region of irrotational flow exists between the two types of layers. On the other hand, when the cylinder is relatively close to the free surface, the two vorticity layers are immediately adjacent to one another and the irrotational region between them is indeed small. In this case, there appears to be an intimate relationship between the unsteady development of each of the two vorticity layers. The evolution of small-scale concentrations of vorticity in each of them appears to occur in a coupled fashion.

It is clear that the vorticity layers originating from the free surface and the upper surface of the cylinder are central to determining the possible states of the wake, which

in turn can be interpreted in terms of vorticity flux, or flow of vorticity, into the near-wake region. A particularly intriguing interpretation of this vorticity flux, arising from two distinctly different sources of vorticity, can be invoked using the same approach for the mixing layer as described by Reynolds & Carr (1985). Employing a simple control volume, which cuts normal to the axis of the jet-like flow, it can be shown that the spatially averaged flux of vorticity $\int u\omega_z dy$ over instantaneous minima and maxima of vorticity, for either the layer originating from the free surface or that from the surface of the cylinder, is approximated well by $U_{avg}^2/2$, in which U_{avg} is the average velocity in the irrotational region, however small, between the two vorticity layers. The consequence of this simple reasoning is that the averaged flux of vorticity in the layer from the free-surface must be the same as that from the surface of the cylinder, which suggests that a compatibility condition must be satisfied: the local curvature of the free surface near separation adjusts to a value such that the vorticity flux from the free-surface matches that from the surface of the cylinder, which has a fixed curvature.

The authors gratefully acknowledge the financial support of the Office of Naval Research under Grants N00014-94-1-1183 and N00014-94-1-0185, monitored by Dr Thomas Swean.

REFERENCES

- APELT, C. J. & WEST, G. S. 1975 The effects of wake splitter plates on bluff-body flow in the range of $10^4 < R < 5 \times 10^4$. Part 2. *J. Fluid Mech.* **71**, 145–160.
- APELT, C. J., WEST, G. S. & SZEWCZYK, A. A. 1973 The effects of wake splitter plates on the flow past a circular cylinder in the range $10^4 < R < 5 \times 10^4$. *J. Fluid Mech.* **61**, 187–198.
- BEARMAN, P. W. & ZDRAVKOVICH, M. M. 1978 Flow around a circular cylinder near a plane boundary. *J. Fluid Mech.* **89**, 33–47.
- DIMAS, A. A. & TRIANTAFYLLOU, G. S. 1994 Nonlinear interaction of shear flow with a free surface. *J. Fluid Mech.* **260**, 211–246.
- GERRARD, J. H. 1966 The mechanics of the formation region of vortices behind bluff bodies. *J. Fluid Mech.* **25**, 401–413.
- HO, C.-M. & HUERRE, P. 1984 Perturbed free shear layers. *Ann. Rev. Fluid Mech.* **16**, 365–424.
- HUERRE, P. & MONKEWITZ, P. A. 1990 Local and global instabilities in spatially developing flows. *Ann. Rev. Fluid Mech.* **22**, 473–537.
- LIGHTHILL, J. 1978 *Waves and Fluids*. Cambridge University Press.
- LIN, J.-C. & ROCKWELL, D. 1994 Instantaneous structure of a breaking wave. *Phys. Fluids* **8**, 2877–2879.
- LIN, J.-C. & ROCKWELL, D. 1995 Evolution of a quasi-steady breaking wave. *J. Fluid Mech.* **302**, 29–43.
- LIN, J.-C., TOWFIGHI, J. & ROCKWELL, D. 1995 Instantaneous structure of near-wake of a circular cylinder: on the effect of Reynolds number. *J. Fluids Struct.* **9**, 409–418.
- MEINHART, C. D., PRASAD, A. K. & ADRIAN, R. J. 1992 Parallel digital processor system for particle image velocimetry. *Proc. Sixth Intl Symp. on Applications of Laser Techniques to Fluid Mech. Lisbon, Portugal, 20–23 (July)*, pp. 30.1.1–30.1.6.
- NEWMAN, B. G. 1961 The deflexion of plane jets by adjacent boundaries – Coanda effect. *Boundary Layer and Flow Control – Its Principles and Application* (ed. G. V. Lachman), vol. 1, pp. 232–264. Pergamon.
- OERTEL, H., JR 1990 Wakes behind blunt bodies. *Ann. Rev. Fluid Mech.* **22**, 539–564.
- REYNOLDS, W. C. & CARR, L. W. 1985 Review of unsteady, driven, separated flows. *AIAA paper* 85–0527.
- ROCKWELL, D., MAGNESS, C., TOWFIGHI, J., AKIN, O. & CORCORAN, T. 1993 High-image-density particle image velocimetry using laser-scanning techniques. *Expts Fluids* **14**, 181–192.

- ROSHKO, A. 1954 On the drag and shedding frequency of two-dimensional bluff bodies. *NACA TN* 3169.
- ROSHKO, A. 1955 On the wake and drag of bluff bodies. *J. Aeronaut. Sci.* **22**, 124–132.
- SHERIDAN, J., LIN, J.-C. & ROCKWELL, D. 1995 Metastable states of a cylinder wake adjacent to a free surface. *Phys. Fluids* **7**, 2099–2101.
- STRYKOWSKI, P. J. & SREENIVASAN, K. R. 1990 On the formation and suppression of vortex ‘shedding’ at low Reynolds number. *J. Fluid Mech.* **218**, 71–108.
- TRIANAFYLLOU, G. S. & DIMAS, A. A. 1989*a* The low Froude number wake of floating bluff objects. Internal Report MITSG89-5, Massachusetts Institute of Technology, Cambridge, Massachusetts.
- TRIANAFYLLOU, G. S. & DIMAS, A. A. 1989*b* Interaction of two-dimensional separated flows with a free surface at low Froude numbers. *Phys. Fluids A* **1**, 1813–1821.
- UNAL, M. F. & ROCKWELL, D. 1987 On vortex formation from a cylinder. Part 2. Control by splitter-plate interference. *J. Fluid Mech.* **190**, 513–529.